May 2022

Potential of Grid-Scale PV and Storage Facilities to Participate in Capacity Markets

Nicholas Giovannetti
University of Wisconsin-Milwaukee

POTENTIAL OF GRID-SCALE PV AND STORAGE FACILITIES TO PARTICIPATE IN CAPACITY MARKETS

by

Nicholas Giovannetti

A Thesis Submitted in

Partial Fulfillment of the

Requirements for the Degree of

Master of Science

in Engineering

at

The University of Wisconsin-Milwaukee

May 2022

ABSTRACT

POTENTIAL OF GRID-SCALE PV AND
STORAGE FACILITIES TO PARTICIPATE
IN CAPACITY MARKETS

by

Nicholas Giovannetti

The University of Wisconsin-Milwaukee, 2022
Under the Supervision of Professor Brian Armstrong

The recent FERC Order 841 has provided an opportunity for grid-scale PV and battery facilities to participate in the capacity market providing ancillary services. Order 841 combined with steadily decreasing PV and battery costs and increasing demand for renewable energy, gives high potential for a PV and battery facility to be economically viable. In this study, an analysis tool is developed as an auxiliary to the PV + Storage + Control + Grid (PSCG) simulation to estimate the megawatts (MW) of dispatchable capacity that can be reliably offered by a PV and storage facility. Limits are based on grid connection, power electronics, and battery energy capacity, and are impacted by variable insolation, load, and system state. The analysis tool visualizes these limitations and economic potential using a Weibull distribution confidence for the results. The study presents a solution that optimizes the PV and battery sizing along with state of charge reserve to give the highest yield given the adjustable parameters with a modular design that can be fitted to look at numerous other parameters that would affect the outcome.

TABLE OF CONTENTS

LIST OF FIGURES

LIST OF TABLES

ACKNOWLEDGEMENTS

First, a thank you to my advisor, Dr. Brian Armstrong, for the opportunity to grow in research and writing under his direction and support. Through two classes, a teaching assistantship, and over a year of working together, you have been invaluable in my growth as a student. You have pushed me towards full potential and I appreciate it more than you know.

Jayme, my love and life, you have supported me every step of the way. Countless late nights of studying, skipped vacations, stress, tears, and more; you have stood by me through the sacrifices and grounded me through it all. I would not be where I am today without your encouragement and support. You have helped me to become a man worthy of your love in personal growth, in character, and ethic.

Thank you to DNVGL for providing Synergi Electric licenses, to WE Energies for their providing feeder data and support, and to GRid-connected Advanced Power Electronic Systems (GRAPES) and NSF for grants and support for the work of the PSCG simulation and completion of this thesis. Also a thank you to Harvey Scribner of Southwest Power Pool as industry liaison support for his expertise and clarity.

To my professors throughout my undergraduate and graduate studies. Kenneth Price and Dennis Rioux of UW-Oshkosh—you kept me afloat for my first year back in school after 10 years of being out and without your help, I don't know if I would have ever got off the ground. Mustafa Farrah, you have become a friend through many years and classes and your standard of teaching and learning helped to shape how I teach and how I learn. Dave McClanahan, a professor and friend, your constant encouragement to think outside the box and not take things too seriously kept a fresh outlook and school and life alike. A thank you to the countless other professors, too many to name, who encouraged the best in not just me, but all students by being true teachers.

To my peers, classmates, and IEEE. No person or student can function alone. It is the individual who puts the work in, but it's those around them that help keep the pace. Late nights in IEEE studying, drawing on the whiteboard, and explaining concepts to each other carried me through so many classes when I couldn't carry myself.

Finally, to my dad. Though you're not here to see it, I admit that I couldn't avoid following in your footsteps. Everything I am today stems from what you taught me of work ethic and of character. I will continue forward, doing my best, knowing that you are proud of me. I am my father's son.

1 Overview

1.1 Introduction

The drastic decrease in price of battery storage and solar photovoltaic (PV) panels coupled with the increasing demand for renewable energies has brought about a need for the ability to accurately predict the performance of grid-scale PV and storage facilities. Additionally, FERC Order 841, published in 2018, provides a way for megawatt-scale facilities to participate in the capacity market. With solar sites needing a great deal of land, many solar sites may be located in remote areas most often serviced by weak feeders. The simulation utilized in this thesis, called PV + Storage + Control + Grid (PSCG), pulls in real feeder data from WE Energies (WE Energies, Personal communication, 2019-2021), real solar irradiance data, and real load data to provide an accurate representation of the grid's response to a PV and storage facility at a site of choice.

The simulation is built using Synergi Electric, utility modeling software provided by DNVGL, and uses feeder data provided by WE Energies to provide accurate site-specific results, as opposed to the more commonly used IEEE standard bus model or Reliability Test System (RTS) model. To enable modeling novel control strategies, Synergi Electric is used to build a database, which is referenced while running the PSCG simulation. This method is then validated against results from Synergi Electric's Time Series Analysis to validate the PSCG simulation results. Using this simulation, multiple parameters are adjusted to view the site's response and voltage levels at the grid connection. These parameters include specific facility sites in the grid, PV sizing [MW], battery power electronic sizing [MW], and battery duration [hours] with multiple control parameters also available, such as reserve state of charge (SoC).

In sizing the facility, the PV is sized by MW, and it is assumed that the battery has its own power electronics. The sizing of the battery is then based on the combined battery power electronics [MW] and the duration [hours] to give total energy in the battery. Therefore, if it is stated the facility has 8MW PV, 8MW battery power, and 4 hour duration, then the total battery energy would be 32MWh with power electronics capable of delivering 8MW. This allows the duration, if held constant, to scale the battery energy by power electronics sizing. Likewise the battery power held constant scales the battery energy by duration.

The results revolve around three core limits of the PV and battery storage facility to provide dispatchable capacity:

1. Limit 1 - The grid's potential to accept power. This is impacted by both MVA and voltage limits, and by the use of reactive power to manage voltage.

2. Limit 2 - Battery power electronics' potential to deliver power into the grid. This is affected by whether the battery is charging or discharging, PV power generation, and possible curtailment.

3. Limit 3 - Defined by the current level of energy in the battery, it is the power that can be delivered over a dispatch duration, taken as the quotient of the battery energy in megawatt-hour (MWh) and capacity contract dispatch duration [hours].

These limits are considered both individually, to examine how changes in the PV, battery power, and duration affect each limit, as well as altogether as an overall minima for potential to deliver power into the grid at a given time. The usefulness of this simulation can be summed up in the question, "If I had X amount of money to invest, how could I split PV and battery to accurately and reliably fulfill a dispatchable capacity contract for X days a year at high confidence." The method for answering this question, posed in this thesis, is covered in depth in a way that utilizes actual site data to confidently predict the outcome, even when the site chosen is on a weak feeder.

The thesis contribution is divided into three distinct areas:

1. Solar irradiance up-sampling

2. Validation of simulation and load tap changer modeling

3. Defining system limits and potential dispatchable capacity

The first two areas directly relate to the simulation completion and the third to dispatchable capacity.

1.2 Thesis Motivation

There are numerous papers that speak to the ability of renewable energy, specifically wind and PV coupled with battery, integrated into a large scale grid to provide arbitrage and dispatchable capacity [22, 23, 24, 25, 26, 28, 29, 30, 32]. Many of these papers do not use actual feeder data in favor of using a standard IEEE bus or a pre-built generic model. This thesis examines the viability of specifically sized PV and storage for dispatchable capacity as a way to generate income through capacity contracts while also considering placement of such facilities on areas with weak feeders, utilizing real feeder, solar irradiance, and load data. The overall motivation of this paper is to demonstrate that the potential for dispatchable capacity

is able to be accurately predicted specific to the location that is chosen while considering limitations of the grid connection, facility sizing, and detailed control policy.

There are papers that optimize sizing based on certain parameters like equipment costs and energy pricing [22, 24, 28] or others that look at multiple batteries distributed in a grid for dispatchable capacity support [23, 30]. The focus of the papers, however, is primarily arbitrage—buying energy at a low price and reselling for higher—rather than a generator such as PV. This additional aspect, PV, increases investment but can be properly modeled to see how and when the capital cost of a generator can be recovered. The novel approach of this thesis breaks down the limitations of a facility at a specific grid location such that the limitation can mitigated or compensated for. Among the papers researched, none consider return on investment (ROI) and facility pricing as a metric for viability. This study uses current pricing of PV and battery storage as well as current energy pricing [22, 28, 31]. The analysis tool produced as the primary contribution of this thesis is unique in that it is coupled to the PSCG simulation to take in a myriad of parameters and produce expected outcomes with high, validated accuracy.

1.3 Thesis Outline

The thesis is divided into two main sections.

- Section 2 - Background Literature
- Section 3 - Research

The background and research are both separated into three sub-sections. First, information is given regarding Synergi Electric and the PSCG simulation's utilization of Synergi Electric. Second, solar irradiance modeling was required for the completion of the PSCG simulation. Lastly, the bulk of the work of both the background literature and research focuses on estimation of dispatchable capacity.

The background is arranged in such a way to walk through the types of regulation, the requirement for dispatchable capacity, market trends and optimization, and resulting in economic potential. With that knowledge in hand, the dispatchable capacity portion of the research is laid out to examine the factors limiting dispatchable capacity, comparing varying parameters that make the dispatchable capacity viable, and reporting the economic benefit.

2 Background

2.1 PSCG Simulation and Synergi Electric

Synergi Electric is a commercial distribution system modeling software utilized around the world and provided by DNVGL. It simulates, analyzes, and plans power distribution feeders, networks and substations [1]. It can contain thousands of elements in a single feeder model and can model feeder-wide impacts such as low and high voltages, losses, load tap changer operation, and load flows. Additionally, Synergi Electric is validated by over 30 years of industry experience.

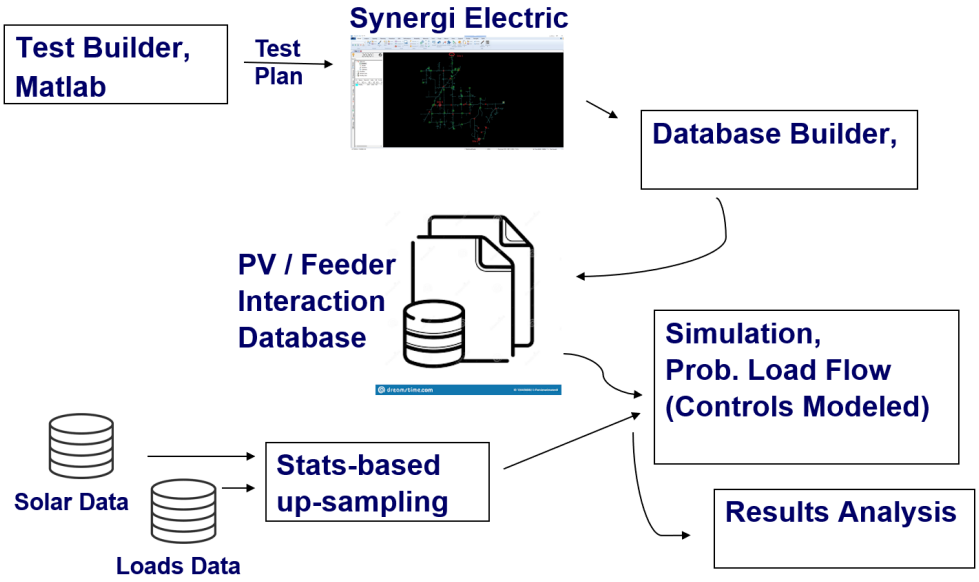

Figure 2-1: PSCG simulation flow with Synergi Electric integration. Adapted from Chatradi *et al.* [2].

A feeder model provided by WE Energies (WE Energies, Personal communication, 2019-2021), shown in Figure 2-2, gives real feeder data for a Wisconsin grid to be used by Synergi Electric for the PSCG simulation. The PSCG simulation utilizes a database built from Synergi Electric's Time Series Analysis tool to produce a high-fidelity, high-resolution modeling of PV and storage deployments [2]. The simulation flow, shown in Figure 2-1 gives a visual representation of how PSCG operates. A test plan is built in Matlab using a sweep of real and reactive power and loads, and is input into Synergi Electric with the feeder model. The results from Synergi Electric, comprised of voltages at the substation and segments throughout the feeder, loading on segments throughout the feeder, and feeder-wide losses, are used to build a feeder interaction database. This database, once built, is then used repeatedly within the PSCG simulation to determine voltage and up to 28 other variables based on real and reactive power at the PV and storage facility and feeder load site.

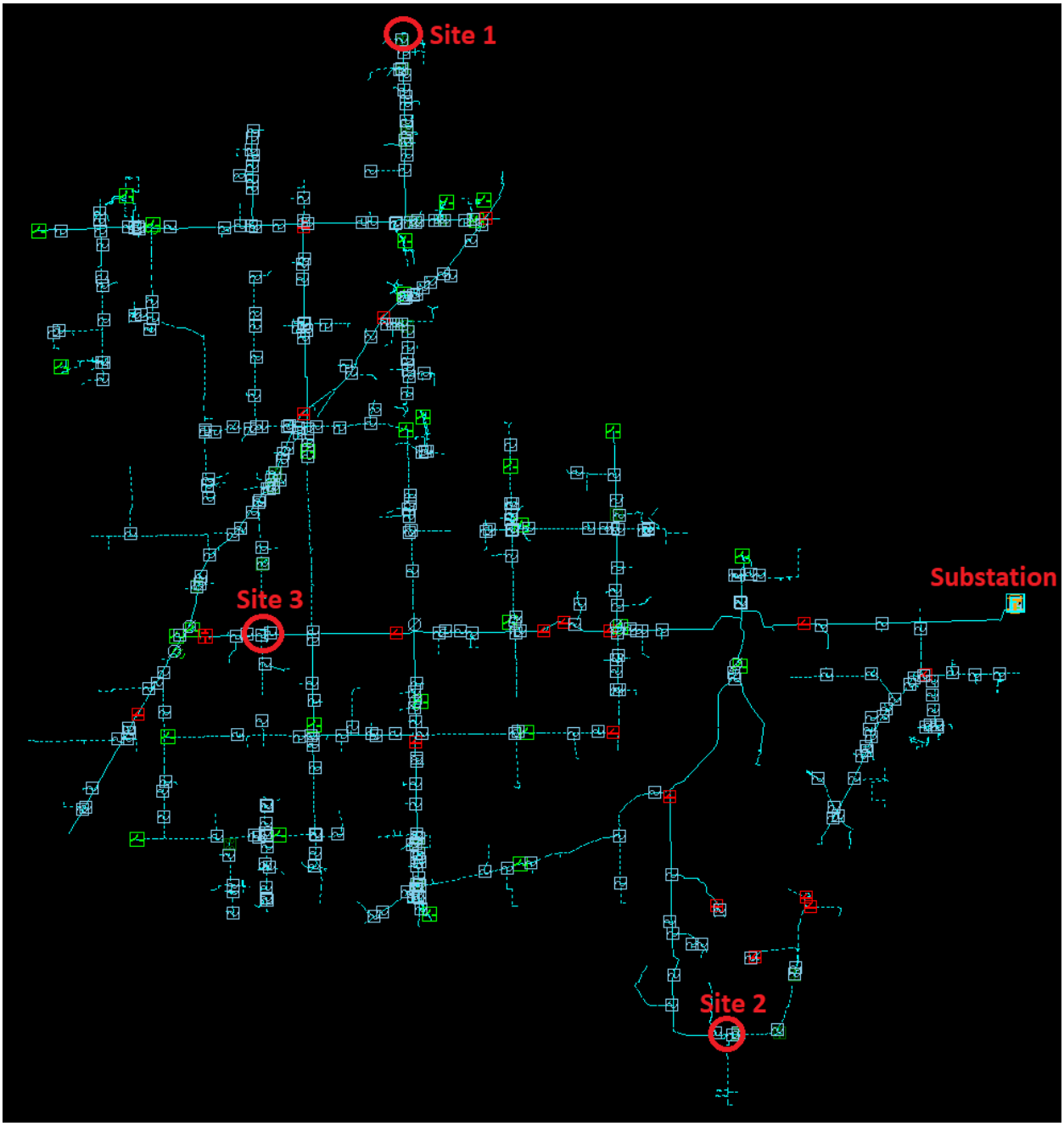

Figure 2-2: Synergi Electric feeder model provided by WE Energies of a real Wisconsin grid.

The sites chosen in Figure 2-2 are candidates for PV and storage facilities with parameters given in Table 5. The benefit of using Synergi Electric for building the database is that Synergi Electric can correctly model complex interactions within the feeder, giving voltages and other values at various points within the feeder.

2.2 Solar Irradiance Modeling

Solar panels rely on semiconductor cells producing photo-current from sunlight. The solar panels are dependent on their exposure to the sun as well as the PV cell temperatures. This points to the importance of modeling the solar irradiance of the area where the PV and storage facility is to be located. The amount of energy produced is proportional to the radiation that reaches the panel, solar irradiance [3]. There are three different aspects of solar irradiation considered in PV effectiveness:

1. Direct Normal Irradiance (DNI)
2. Diffuse Horizontal Irradiance (DHI)
3. Global Horizontal Irradiance (GHI)

DNI is the term for direct radiation that reaches a panel and is of interest to concentrated solar that would track the sun's position, maximizing captured radiation. DHI is a scattered irradiation which is due to the sky and fractional cloud cover. This value changes slowly in relation to DNI and GHI but also decreases when a panel is tilted rather than horizontal (normal to the sky). GHI is a combination of DNI and DHI for a horizontal panel such as a photovoltaic [35]. The GHI is given as

$$\text{GHI} = \text{DNI} \cdot \cos(\theta_s) + \text{DHI} \tag{1}$$

where θ_s is the zenith angle, the angle at which the sun is relative to the normal of the panel. Solar zenith angle is specific to the latitude of the PV facility [36],

$$\begin{aligned} &\cos(\theta_s) = \sin(\alpha_s) = \sin(\Phi)\sin(\delta) + \cos(\Phi)\cos(\delta)\cos(h) \\ &\text{where} \\ &\theta_s \text{ is solar zenith angle} \\ &\alpha_s \text{ is solar altitude angle where } \alpha_s = 90^\circ - \theta_s \\ &h \text{ is the local hour angle in solar time} \\ &\delta \text{ is current local declination of the sun} \\ &\Phi \text{ is local latitude} \end{aligned} \tag{2}$$

This is the benefit of getting real solar data, in that the zenith angle can be calculated based on the location and correlated to the irradiance values. The up-sampling of the solar irradiance can be done by simply interpolating between points. However, this does not take into account the high-frequency cloud cover

since the short-term changes of the solar irradiance dramatically affect power generation [17]. A battery can help to smooth out cloud cover changes but, it is desirable to model the solar irradiance on the same time scale as the simulation to accurately simulate the real PV response. Since the GHI is proportionate to the amount of cloud cover, okta is a prime candidate as a way to simplify the approach to up-sampling the solar irradiance data. Okta is a representation of cloud cover in 9 increments, from 0 to 8, with 0 being completely clear and 8 being completely covered by cloud. Okta value is considered an acceptable representation of obscured irradiance once adapted [12]. Among many stochastic approaches to up-sampling solar data, a Markov chain is well established as an acceptable method for modeling solar irradiance [8, 9, 12].

2.2.1 Markov Chain Modeling

A Markov model is used as a stochastic method to generate the statistically valid up-sampled elements of the solar irradiance. The benefit of the Markovian process is that it's probabilistic and the transition of one state to the next is only dependent on the current state [5]. The probability of the future state is directed by discrete probabilities from prior events [12]. In this case, ground measurements can be derived from satellite images to obtain hourly or sub-hourly GHI, DHI, and DNI. The 30-minute data can then be used with the Markov model to synthesize statistically valid one-minute okta values.

The Markov model relies on a transition probability matrix (TPM) constructed of discrete states based on an adequate amount of past samples. Bright *et al.* and Ngoko *et al.* both outline the construction of the TPM [12, 13]. The transition probability matrix is given as

$$\begin{aligned} P_{ij} &= P(X_t = j | X_{t-1} = i, X_{t-2} = i_{t-2}, \ldots, X_0 = i_0) \\ &= P(X_t = j | X_{t-1} = i) \end{aligned} \tag{3}$$

where P_{ij} is the transition probability from state i to j represented as

$$P = \begin{bmatrix} P_{11} & P_{12} & \ldots & P_{1s} \\ P_{21} & P_{22} & \ldots & P_{2s} \\ \vdots & \vdots & \ddots & \vdots \\ P_{s1} & P_{s2} & \ldots & P_{ss} \end{bmatrix} \tag{4}$$

where i and j of Equation (3) are present to future okta numbers, respectively. In the case of the application of okta, the number of states is 0-8 represented as 1-9 in the TPM equation. An appropriate amount of data should be used to build the TPM. Bright *et al.* uses 10 years and Ngoko *et al.* uses 2 sets of 3 years of data.

Wind speed, pressure, and cloud height can be used along with okta for more accurate modeling [12].

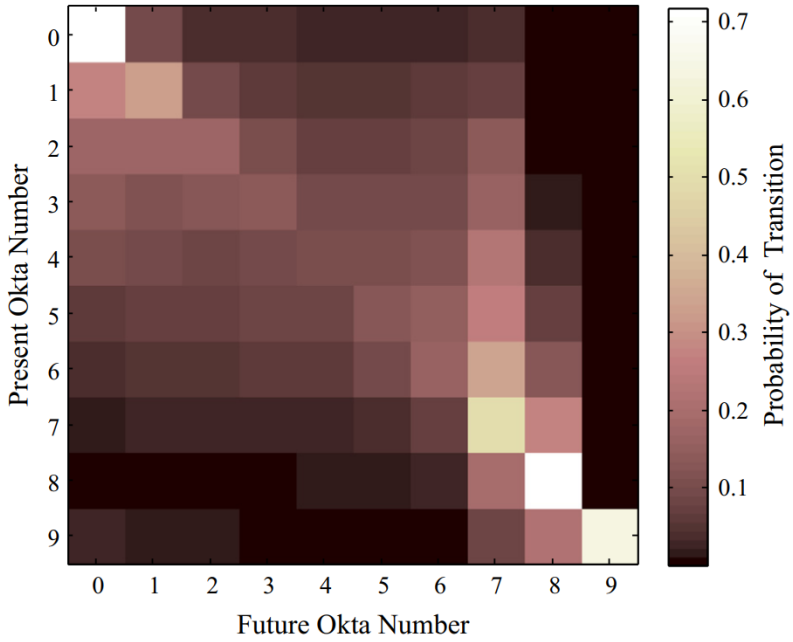

Figure 2-3: Colour plot illustrating the Markov chain for the mean annual transition probability of okta number from the present hour to the future hour. Adapted from Bright *et al.* [12].

Figure 2-3 shows the resultant transition probability matrix for okta used to predict changing cloud cover. In this case, another okta value of 9 is added, which is a special case where the cover is fog rather than cloud cover [12]. The TPM makes reasonable sense as there is significantly lower probability to go from no cloud cover at all to fully covered, with increasing probability to transition to a state only 1 away from the current. For simplicity of the modeling, a single order transition matrix is used, though it is not uncommon to use higher order [12, 13].

The future state $X(t)$ can be generated by picking a random number r with normal distribution of 0 to 1 and mapping it to the corresponding cumulative distribution vector $F(t)$ [13],

$$F_h(t) = \sum_{i=1}^{h} P_i(t) \tag{5}$$

where row i of the probability matrix is taken for the current okta, and h is the h^{th} entry in F(t) using the transformation with number of samples, s,

$$X(t+1) = \frac{1}{s}\left\{(i-1) + \frac{r - F_{i-1}(t)}{F_i(t) - F_{i-1}(t)}\right\} \tag{6}$$

In application, the random number generated can be used as a weight to choose the next okta value by utilizing the TPM generated from previous data. For each sample, the okta value associated with the specific day can be generated by prior years of data accounting for seasonal differences of GHI .

2.3 Dispatchable Capacity Provision

2.3.1 Regulation Services

Distributed energy storage can be used to support ancillary services and operating reserves within the grid to generate revenue. Battery energy storage systems (BESS) that operate in strictly arbitrage systems—buying energy at a time of low cost and selling when higher—currently make up significantly less of the utility-scale BESS in the grid[20]. The additional PV with battery alleviates the need to purchase energy from the grid at a lower cost but rather relies solely on solar to charge the batteries during the day. Ancillary services are split into three regulation levels:

1. Primary - Response time of 0 (instant) to 30 seconds, without human intervention
2. Secondary - Response time of tens of seconds to approximately 200 seconds
3. Tertiary - Minutes to respond, generally up to 15 minutes

Among operating reserves and ancillary services, different categories exist that a PV and battery storage facility can operate in, especially primary, shown in Table 1. Listed operating reserves such as frequency response, regulation, and contingency spinning reserves are prime candidates for PV and battery storage systems as they require a fast response but have generally low durations of service. Another benefit of a PV and battery facility is that they can respond instantly with no human interaction which is a requirement of frequency regulation. This makes it an ideal choice for spinning reserves, particularly frequency regulation since the response can be determined by control laws [32].

Table 1: Applications of Utility-Scale Energy Storage. Adapted from Bowen *et al.* [7].

Application	Description	Duration of Service Provision
Arbitrage	Purchasing low-cost off-peak energy and selling it during periods of high prices.	Hours
Firm Capacity	Provide reliable capacity to meet peak system demand.	4+ hours
Operating Reserves • Primary Frequency Response	Very fast response to unpredictable variations in demand and generation.	Seconds
• Regulation	Fast response to random, unpredictable variations in demand and generation.	15 minutes to 1 hour
• Contingency Spinning	Fast response to a contingency such as a generator failure.	30 minutes to 2 hours
• Replacement/Supplemental	Units brought online to replace spinning units.	Hours
• Ramping/Load Following	Follow longer-term (hourly) changes in electricity demand.	30 minutes to hours
Transmission and Distribution Replacement and Deferral	Reduce loading on T&D system during peak times.	Hours
Black-Start	Units brought online to start system after a system-wide failure (blackout).	Hours

The different tiers of regulation generally go in order as the grid needs. Primary is activated first to accommodate sudden, unpredictable changes, then secondary is activated if the grid continues to need support such as a contingency, while tertiary are called upon to further assist the grid in a case such as a generator outage. The benefit of a BESS is that it can value-stack. Since ancillary service bids are rarely called upon to be dispatched [22], a PV and battery system can operate in reserve services and voltage regulation while holding energy in reserve for high-value capacity contracts [20].

2.3.2 Developments in Independent Storage

The US Department of Energy published the United States Electricity Industry Primer in July 2015 [19], defining the need for grid operators to ensure load services are able to meet an expected demand plus a "reserve margin." This has led to the creation of the capacity market which will use auctions to lock in a price up to 3 years in advance [19]. The capacity market pricing varies by ISO but not typically by contract offers. FERC Order 841 issued in 2018 establishes a participation model of market rules that recognize physical

and operational characteristics of electric storage resources to facilitate participation in ISO markets [18]. This gives way for independent, privately owned PV and storage facilities to participate in the capacity market regardless of their overall size and capacity offering. The caveat is that different ISO's can enforce a minimum duration by derating the price proportional to the minimum [26].

Among the market rules are introduced parameters such as time dependent pricing to cover high-load times as well as the ability to provide a spinning reserve. An example chart of average clearing price from California Independent System Operator (CAISO) is given in Figure 2-4 [22].

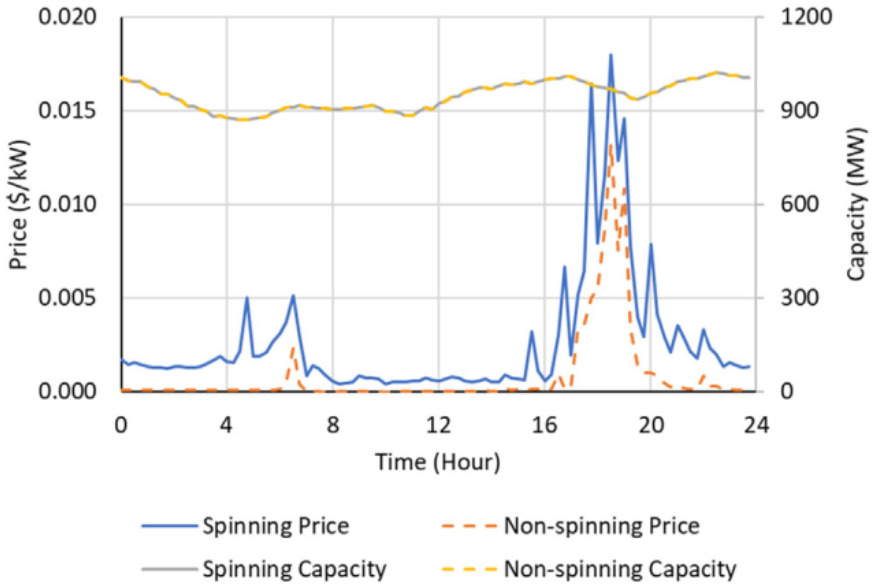

Figure 2-4: Average annual required capacity and clearing price for the spinning and non-spinning reserve ancillary service markets in CAISO. Adapted from Nelson *et al.* [22].

The increased price shown at the end of the day correlates to high load times, typically from 4pm-10pm. Also seen is the benefit of participating in spinning reserves to generate a higher return. The spinning price is nearly always higher since the generator must be online and synchronized to respond quickly. A spinning reserve refers to an unloaded, synchronized resource that is deployable in 10 minutes or less [27]. A spinning reserve is generally used in the case of a frequency decay due to high load. The total amount of spinning reserve in a system should be sufficient to cover the loss of the largest unit [3]. With the increased value to providing capacity contracts for holding reserve power, the value-stacking FERC Order 841 provides makes PV and battery sites viable for quicker returns.

For this study there is a focus on the specific Independent Service Operator (ISO) that governs Wisconsin since that is the site location chosen. The Midcontinent Independent Service Operator (MISO) covers Iowa, Minneapolis, and Wisconsin with portions of Arkansas, Indiana, Louisiana, Michigan, Minnesota, Mississippi,

Missouri, Montana, and Texas. The focus of the dispatchable capacity has been chosen to be the same area of the grid model provided by WE Energies. MISO's 2021 average pricing for ancillary generation regulation closed at $360/MW-day, in line with reported pricing in cited papers focused on dispatchable capacity [22, 28].

Looking ahead to future viability for PV and battery facilities, the MISO 2020/2021 Planning Resource Auction (PRA) Results outlines the year's closing auction prices for dispatchable capacity along with trends of energy distribution. Renewable energy supplies a low portion of the overall fuel types contributing to the 136GW of power at 3.04%, with only 0.64% contributed from solar. However, the focus of fuel type shifted dramatically towards renewable energy between 2019-2020 and 2020-2021. Solar and wind energy each rose over 20% which is a considerable increase in relation to other fuel types only changing in single-digit percentages [21].

Table 2: MISO 2020-2021 PRA Fuel Type. Adapted from MISO [21].

Planning Year	**2019-20**		**2020-21**		**Change**	
GADS Fuel Type	**System (MW)**	**% Fuel**	**System (MW)**	**% Fuel**	**Delta (MW)**	**Delta (%)**
Coal	47,059	34.93%	46,576	34.25%	-483	-1.03%
Gas	51,317	38.08%	52,247	38.42%	930	1.81%
Nuclear	12,274	9.11%	12,034	8.85%	-240	-1.96%
Load Modifier(DR/EE)	7,722	5.73%	8,208	6.04%	486	6.29%
Water	6,176	4.58%	6,021	4.43%	-155	-2.51%
Oil	3,528	2.62%	3,411	2.51%	-117	-3.32%
Wind	2,698	2.00%	3,275	2.41%	577	21.39%
Waste Heat	1,125	0.83%	1,204	0.89%	79	7.03%
Other-Solid(Tons)	814	0.60%	838	0.62%	24	2.89%
Distillate Oil	604	0.45%	582	0.43%	-22	-3.58%
Other-Liquid(BBL)	49	0.04%	48	0.04%	-1	-1.43%
Other-Gas(CuFt)	553	0.41%	542	0.40%	-11	-2.06%
Wood	144	0.11%	143	0.11%	-1	-0.76%
Solar	680	0.50%	850	0.63%	170	25.06%
SYSTEM	134,743	100%	135,978	100%	1,235	0.92%

2.3.3 Market Trend of PV and Battery

The ongoing trend of yearly increasing renewable energy, especially solar, is in part due to the trend of decreasing cost of solar and battery over the last decade. Battery prices, specifically lithium-ion, have

decreased 88% in the last decade, with the last three years being approximately 14% per year [26, 31]. Figure 2-5 shows the forecast of battery pricing to continue to decrease to near-half values in the next several years. This is backed up by earlier projections of battery pricing now matching with what is current, such as Curry's prediction in 2017 of current 2021 battery pricing [4].

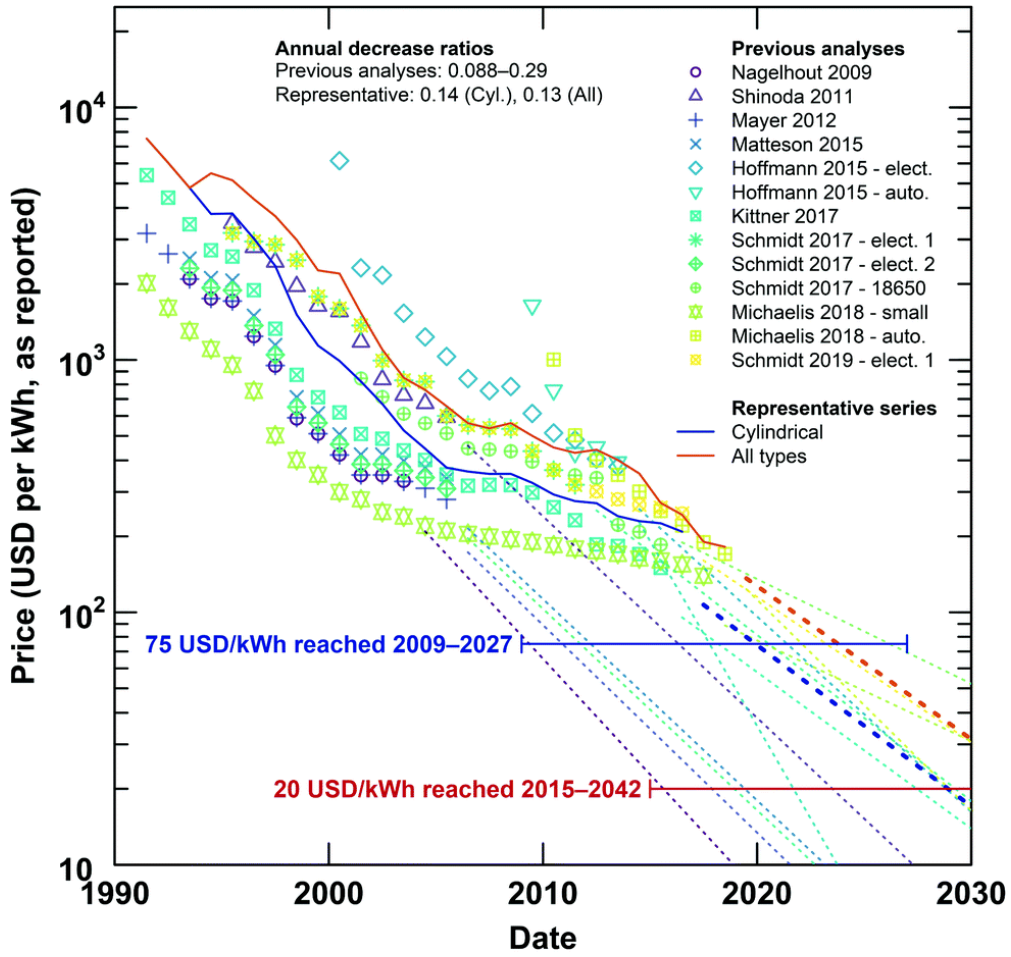

Figure 2-5: Extrapolated forecast of battery pricing trending. Adapted from Ziegler and Trancik [31].

Likewise, PV cost has decreased 81% in the last decade with consistent 13-18% yearly decreases over the last few years, shown in Figure 2-6. This comes coupled with the increasing demand of renewable energies among generation resources in the US. The overall trend of increasing demand and decreasing price has led to numerous studies of battery installations for ancillary services [22, 26, 28, 29, 32].

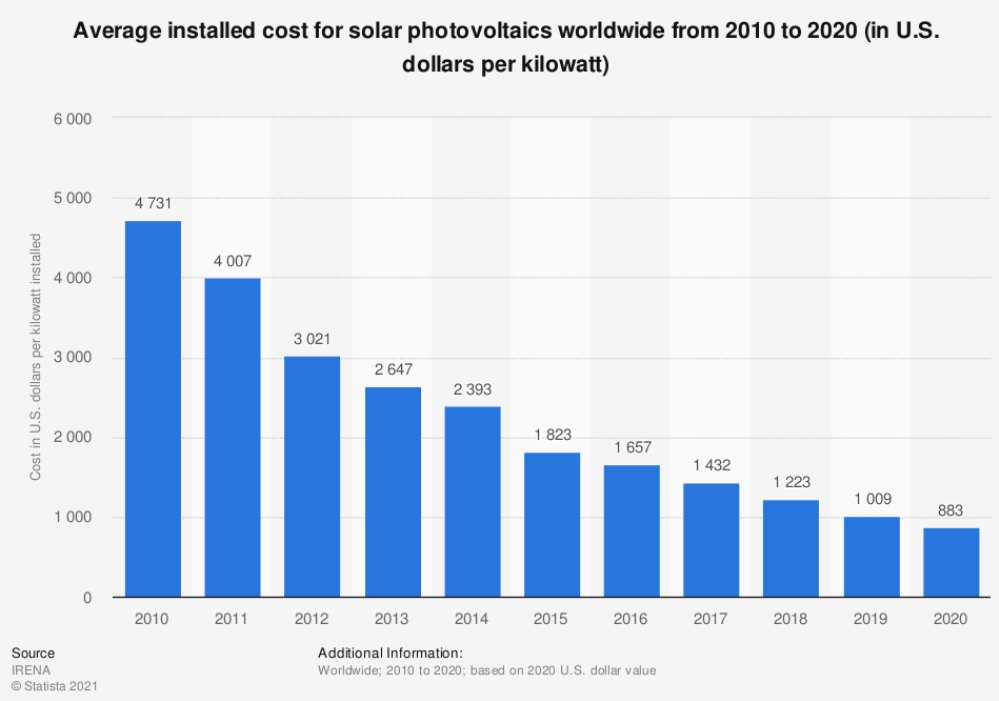

Figure 2-6: Average installed cost for PV from 2010 to 2020, $/kWh. Adapted from Jaganmohan [34].

2.3.4 Optimization of PV and BESS for Ancillary Markets

Examining several sources for what is currently recommended for ancillary markets, a common approach has become to scale the battery storage and PV to an optimal rating that can provide a balance between cost and yield.

Control Law

Nelson *et al.* demonstrates the effectiveness of model predictive control with cost analysis for increased revenue generation [22]. While the facility is a microgrid rather than utility scale, the detail of analysis in the revenue based solely off control method is convincing. The study examines the effectiveness of reserve state of charge (SoC) for ancillary service markets and the reduction in operating expenses when participating in the ancillary market. The introduction of model predictive control (MPC) over logic-based control was shown to give a 13.73% increase in revenue. The benefit of the MPC control is that the charging and discharging of the battery can be managed by an objective function comprised of variable costs with constraints to keep a minimum in the battery for ancillary support. This is similar to what is done in the research of Section 3.3.

In Nelson *et al.* [22], the objective function is comprised of a compensation price and dispatchable capacity for both spinning and non-spinning reserve, as well as cost for replacement reserve into grid. The ancillary service portion is treated as strictly revenue and is a reducing objective function. Constraints are

put in place for energy asset specifications, load forecasts, and renewable energy forecasts that ensure the load is served by power generated or power purchased from the grid. The ability to specify the amount of energy that can be curtailed is built into the constraints as well as upper and ramping limits of the generator, as to be expected. The constraint of interest in this case is the minimum reserve SoC and maximum of the energy level in the battery storage, ensuring that the spinning reserve capacity can be met if called upon. This provides the ability to enter capacity markets and ancillary services. Also considered in this constraint are the operational limitations of the PV and battery.

Real load and solar data from the university of study (ASU Fulton Center) was collected to size the battery and PV to meet maximum demand within the microgrid with a diesel generator included as a backup. Since the PV is sized to meet maximum demand, the facility produces more power than the microgrid consumes 27.4% of the time with excess being sold back to the grid at wholesale rate, shown in Figure 2-7. The excess energy sold at wholesale pricing helps to offset operational costs and add to the revenue of the ancillary services.

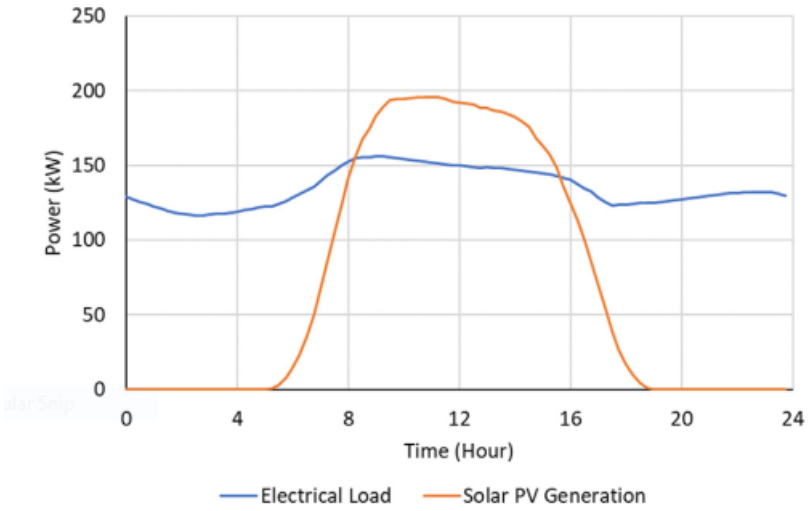

Figure 2-7: Average annual electrical load and on-site solar PV generation of the ASU Fulton Center. Adapted from Nelson *et al.* [22].

The outcome of Nelson *et al.* not only shows the benefit of model predictive control for optimizing a PV and battery facility, but it also points to the benefit of using the control law to manage reserve SoC in the battery to operate in a profitable ancillary service market. While the grid operated with higher energy sales due to excess energy with a simple logic based controller at 67%, participation in the ancillary service markets increased total revenue by 354%—a four-fold increase over other control strategies that focus on energy sales only.

Strengths of Nelson's paper and similarities to this study include the consideration of facility limits and minimum reserve SoC for the provision of dispatchable capacity into the grid. Another strength is the detailed simulation considering different costs and timings to show revenue change. The addition of the MPC only further validates the benefit of ancillary service participation. A weakness in this paper is the aspect of the microgrid. With a non-utility-scale application, total loads and grid connection capacities are irrelevant to the productivity of the PV and battery facility. Related to the microgrid, another weakness is that the facility in question is limited to generation and consumption within its own location, the ASU Fulton Center, and sizing the PV is done solely to meet the microgrid's demand. There is readily available high resolution load and solar data gathered at the location, the latter being not easily obtained elsewhere. There is also the issue of yearly yields only considered as decreases in the operating costs of the location, rather than a yearly yield versus cost showing ROI.

Capacity Value

Sioshansi *et al.* and Madaeni *et al.* are considered as a pair for their work on capacity value estimation for both PV and energy storage facility locations [23, 25]. Sioshansi adds dynamic programming to the capacity evaluation to improve the charging and discharging rates and state of charge reserve. Published in 2013 prior to FERC Order 841, both seek to solve the issue of generator outage support and energy arbitrage by evaluating the optimal charging and discharging rate and levels of an energy storage system within the grid. In Sioshansi's paper, five utility systems are examined, Pacific Gas and Electric (PGE), Southern California Edison (SCE), NV Energy (NE), Public Service Company of New Mexico (PNM), and FirstEnergy (FE).

The system uses energy pricing based solely on arbitrage. A normal strategy for arbitrage is to charge the batteries during times of low energy cost and discharge at the highest offer price [22, 23, 25, 29, 32]. This leaves a gap in the times that energy price is on a downward trend after its peak. Assuming most dispatchable capacity systems have discharged their power after the high price, any system outage would cause a deficit in energy reserves. This is shown in Figure 2-8a comparing the energy price to loss of load probability (LOLP) and probability of shortage, ϵ.

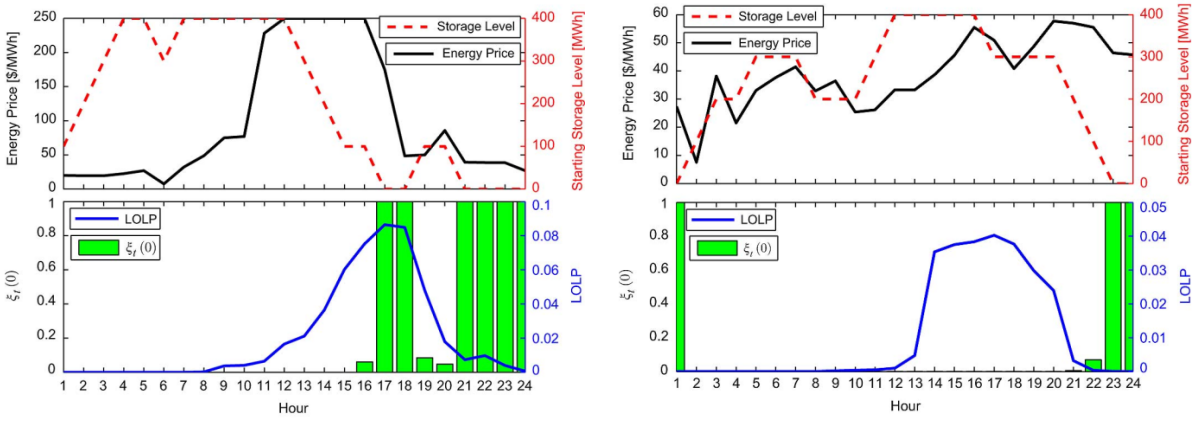

Figure 2-8: (a) Hourly energy prices, LOLPs, and storage dispatch in PGE system on July 12, 1999 (b) September 9, 2004. Adapted from Sioshansi *et al.* [23].

The solution is keeping the energy price level with only a slightly higher price at times of high load, shown in Figure 2-8b. A leveled energy price keeps dispatchable capacity readily available after times of high energy price. This is further applied in later years when dispatchable capacity ancillary services are more common than systems using strictly arbitrage [28]. Additionally, the pricing model shown is more similar to current dispatchable capacity pricing than wholesale energy pricing. Sioshansi *et al.* points to the importance of real-time capacity markets having a coincidence with LOLPs as they are more up-to-date with grid capacity levels. A weakness in this approach is that the optimization criteria is strictly based on energy-based profit maximization rather than the grid's real capacity value at a given time [23]. Denholm *et al.* expounds on this with the systems equipped for both arbitrage and ancillary services to maximize revenue [28], supported by Nelson *et al.* and others [22, 32].

Sioshansi *et al.*, however, fail to take into consideration grid connection capacity limits which would prevent dispatchable capacity from operating in the market, even at times of high LOLP. Another aspect is that the dynamic programming only helps to size the dispatchable capacity minimally rather than over-sizing. This works to provide the need for a capacity market that can support throughout high load and loss areas, but is less applicable to PV and battery storage that would provide a contribution to the need —most likely smaller than the 100MW facilities that are recommended.

Madaeni *et al.* helps to bridge the gaps of Sioshansi *et al.* by providing an argument for capacity value in PV facilities [25]. The case study is comprised of 14 locations in the western U.S. with 100MW PV plants at each location. Madaeni *et al.* uses only PV rather than PV and battery facilities. A fixed load is applied based on hourly load data for each site, scaled by year. The PV model used is the 2011.6.30 National Renewable Energy Laboratory's Solar Advisor Model (NREL SAM) and takes in weather data

including solar irradiation to simulate hourly net electrical output. This method also accounts for losses and parasitic loads.

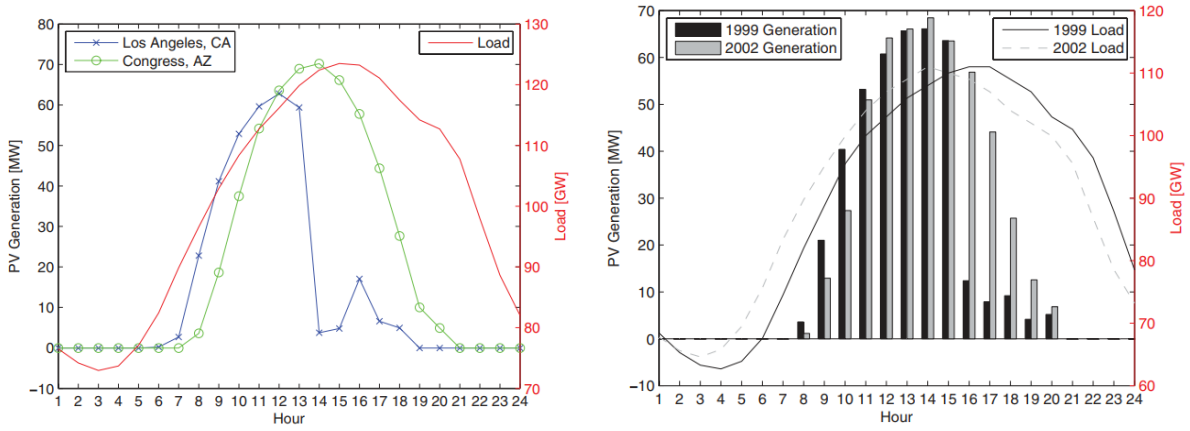

(a) (b)

Figure 2-9: (a) Hourly loads and output of a fixed-axis PV plant located in Los Angeles, CA, and Congress, AZ, on July 20, 2005 (b) Congress, AZ, on July 12, 1999 and July 10, 2002. Adapted from Madaeni *et al.* [25].

The study is structured to show the importance of location and seasonal data in answering the capacity value question. Figure 2-9 shows average hourly generation for each of the three sites. Figure 2-9a shows the differing solar generation between Los Angeles, CA and Congress, AZ. This factor of differing generation shows the importance of site-based study in overall dispatchable capacity estimation. Using real site data for a given location for each case study gives a better view of reliability and is proven in other papers as well [22, 29]. Figure 2-9b supports the use of multiple years of data, as the generation of a single site (Congress, AZ) is significantly different between two sample years. In this case, using only an average of solar generation will over-estimate in one year and under-estimate in another.

Likewise, the change in generation from year-to year supports the use of battery with PV generation to capitalize on high yield energy sales from increased load times [22, 23]. The addition of battery also helps to mitigate curtailment when the system is generating more than the grid can support, something Madaeni overlooks in the capacity value study. Madaeni *et al.* also admittedly points to the need for localized, site-specific data for load and solar irradiance. All this considered, there is a strong case in both Sioshansi *et al.* and Madaeni *et al.* for the value of dispatchable capacity in current markets and the importance of real data used for the analysis.

2.3.5 Economic Potential of Dispatchable Capacity in Reserve Markets

Frazier *et al.* use a Regional Energy Deployment System (ReEDS) linear optimization model comprised of 134 load balancing areas across the United States to asses the potential of battery storage as a capacity resource [26]. The study focuses primarily on short term ancillary services such as frequency regulation but cites FERC Order 841 [18] as a motivation for the study. The size and duration of the batteries are optimized based on current pricing and future predictions through 2050. Also stressed by Frazier *et al.* is the importance of adjusting minimum durations to avoid unserved energy while also considering battery capital costs.

Battery durations of 2, 4, 6, 8, and 10 hours are tested for optimization. The ReEDS model plans the mandates of storage by 2030 with included modifications for battery energy sizing as well as constraints for reliability to account for seasonal changes in PV generation. The simulation processes 1 day from each season with 4 time intervals: morning, afternoon, evening, and night, as well as a single afternoon in summer. The simulation sizes each duration based on the battery capacity and the resource adequacy contribution, which takes into account capacity credit derated due to insufficient duration. ISO's may impose a minimum duration for capacity contracts with a penalty based on offered duration versus minimum. For example, there may be a 4-hour duration minimum for an ISO, so a 2-hour duration contract would be derated by $\frac{1}{2}$ the standard price. Results shown in Figure 2-10 show that 2-hour batteries provide a considerable amount of dispatchable capacity but operate at nearly 60% equivalence due to derating based on duration.

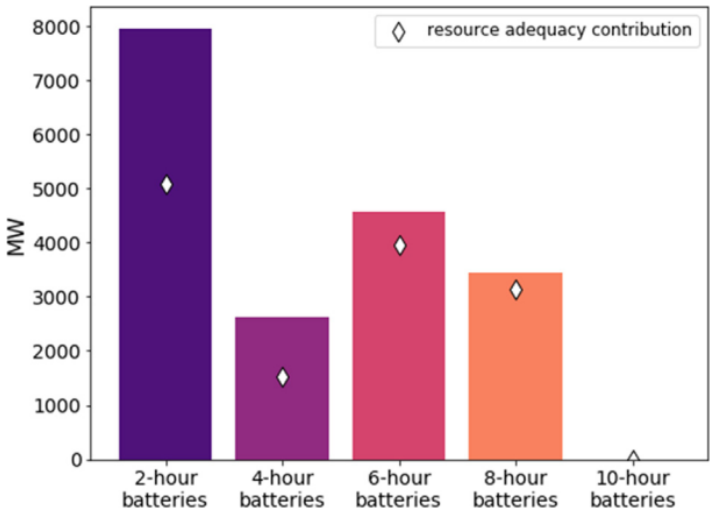

Figure 2-10: Installed battery capacity and resource adequacy contribution (capacity derated by capacity credit) in ReEDS. Model results for ERCOT in 2050. Adapted from Frazier *et al.* [26].

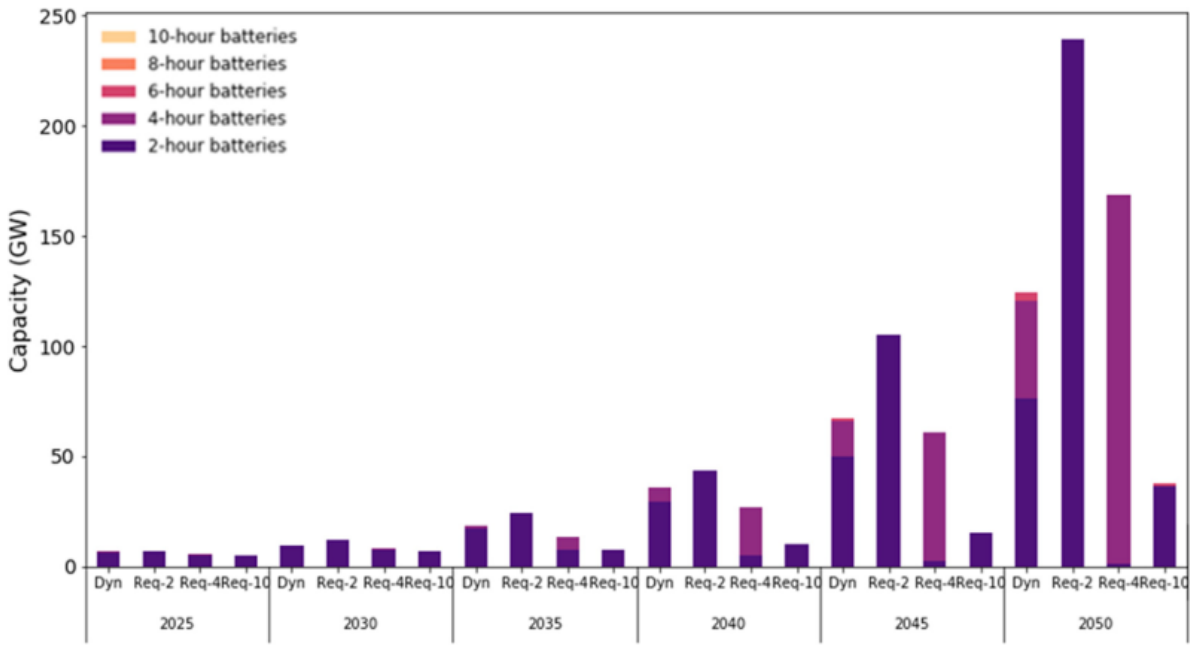

Figure 2-11: Cumulative battery storage deployment by duration over time with two-, four-, and ten-hour duration requirements (Req-2, Req-4, and Req-10) for full capacity credit, compared to the Reference dynamic storage capacity credit scenario (Dyn). Adapted from Frazier *et al.* [26].

Frazier *et al.* also predict a steep decline in battery costs from 2020 to 2030 at 26%, with a total decrease in cost of 50% by 2050, making a case for larger battery deployment. The simulation shows a steadily increasing demand for 2-hour batteries, even at a derated return, due to prospective higher PV penetration to serve peak demand. This ties in with the benefit of PV and battery coupled together, as Frazier *et al.* mention that areas of higher PV and wind penetration provide an economic advantage of batteries since they can provide flexibility in the system. With the combined PV and wind penetration, the ReEDS model shows potential for dispatchable capacity in the U.S to exceed 100GW by 2050 for batteries of 10-hours or less.

Frazier *et al.* alleviate concerns of over-saturation of the currently small capacity market with a considerable amount of dispatchable capacity ancillary services by 2050, shown in Figure 2-11. It doesn't answer the question of site-specific data as it is too broad, which is what this thesis seeks to cover. It does, however, give valuable information of expected battery energy sizing, ISO duration constraints, and a long-term view of dispatchable capacity viability at the current rate of expansion.

A separate study by Sioshansi *et al.* seeks to estimate the value of energy storage for arbitrage and ancillary services [24]. The study, done in 2008, is prior to FERC Order 841 and does not consider the ease of independent PV and battery facilities to participate in capacity markets. Sioshansi *et al.* instead seek

to optimize the battery duration by arbitrage value. Results show the knee of curve at 8-hours duration for value of arbitrage, shown in Figure 2-12. Assumptions are made of transmission efficiencies but it is acknowledged that energy prices and transmission constraints will vary by location. The solution to the variation, of course, is simulating the effects for each location but Sioshansi *et al.*, like others, agree that logically charging and discharging due to regional differences in energy availability is key to optimizing the facility performance [22, 26, 32].

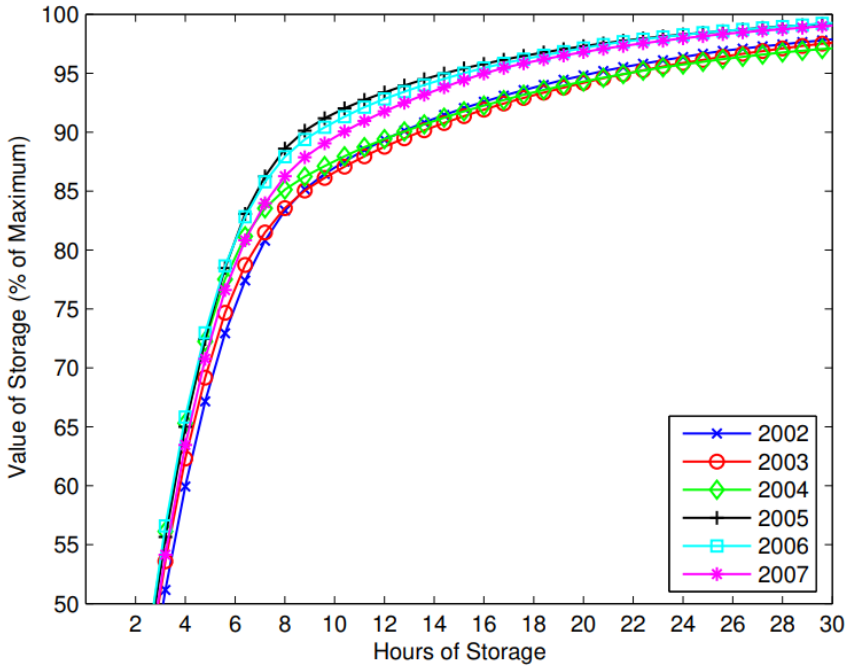

Figure 2-12: Potential annual arbitrage value captured, as a percentage of maximum theoretical value. Adapted from Sioshansi *et al.* [24].

Sioshansi *et al.* focus on arbitrage, but a portion is dedicated to the benefit of ancillary services as a way to motivate capacity contracts where price caps limit energy arbitrage prices. This is supported by a later paper from Sioshansi *et al.* as well [23]. The value, Sioshansi *et al.* say, is in co-optimizing the different markets like arbitrage and ancillary services, even though at the time of the study it was difficult to predict long term benefits of ancillary services, they are most likely substantial. Recent developments such as FERC Order 841 prove Sioshansi *et al.* were correct. A consistent focus of the paper is the apparent shift away from arbitrage as the energy prices change and dispatchable capacity adapts. The analysis of dispatchable capacity must be multi-faceted, considering multiple attributes and interplay of sources to avoid underestimating the value of energy storage; this includes contract, market structure, and cost of ownership.

Padmanabhan *et al.* cite the recent FERC Order 841 as a driving factor for their study of BESS

in energy and reserve markets, focusing on a combination of arbitrage and ancillary service support while considering reserve SoC, charging rates, and yield [30]. The operational cost function model proposed consists of degradation cost based on charging/discharging rates, depth of discharge (DOD), and a spinning reserve cost. DOD refers to the energy discharged from the battery relative to its maximum charge. This model seeks to justify the cost to yield ratio of participating in both arbitrage and ancillary markets. The facility's physical and operational characteristics must coincide with Order 841 in that the discharge structure must be adequate to enter the capacity market. In this case, an hour of operation is set as a minimum for entry into the capacity market,

Like in prior studies [22, 26], Padmanabhan *et al.* consider co-optimizing energy sales and ancillary services to maximize yield of a facility. The balance between wholesale energy sales and ancillary services is that reserve SoC for ancillary services forgoes the opportunity of a portion of wholesale energy sales. No assumption is made of the dispatchable capacity bid/offers but rather is left as a flat percentage. The optimization is then tested on the IEEE Reliability Test System (RTS) including multiple generators, loads, transmission lines, and batteries. In Padmanabhan *et al.* three cases are studied [30]. Case 1 is a base case without BESS participation, case 2 is with BESS with a simple bid/offer model, and case 3 is BESS participation with their proposed bid/offer model taking into account degradation.

Table 3: All day Aggregate Market Clearing Results. Adapted from Padmanabhan *et al.* [30].

	Case 1	**Case 2**	**Case 3**
Energy cleared (MWh)	67,923	67,984	68,079
Generation dispatch (MWh)	69,928	69,059	69,121
BESS charging energy (MWh)	-	331	301
BESS discharging energy (MWh)	-	299	272
Losses (MWh)	1,005	1,043	1,013
BESS charging cost ($)	-	17,907	13,427
BESS degradation cost, CI ($)	-	-	8,069
BESS spinning reserve cost ($)	-	7,582	7,831
BESS energy market revenue ($)	-	23,115	18,005
BESS spinning reserve market revenue ($)	-	15,979	16,143
BESS profit ($)	-	13,084	10,821
Social Welfare ($)	4,716,866	4,769,135	4,773,927

The simulation shows two important factors in Table 3. First, there is substantial revenue gained from

participating in both wholesale energy and ancillary services. Second, the degradation cost, which is a factor of DOD and charging/discharging rate, can have a substantial impact on the cost and longevity of the system. It should also be noted that managing parameters like DOD and charging/discharging rates extends the life of the batteries, thus providing more income over time.

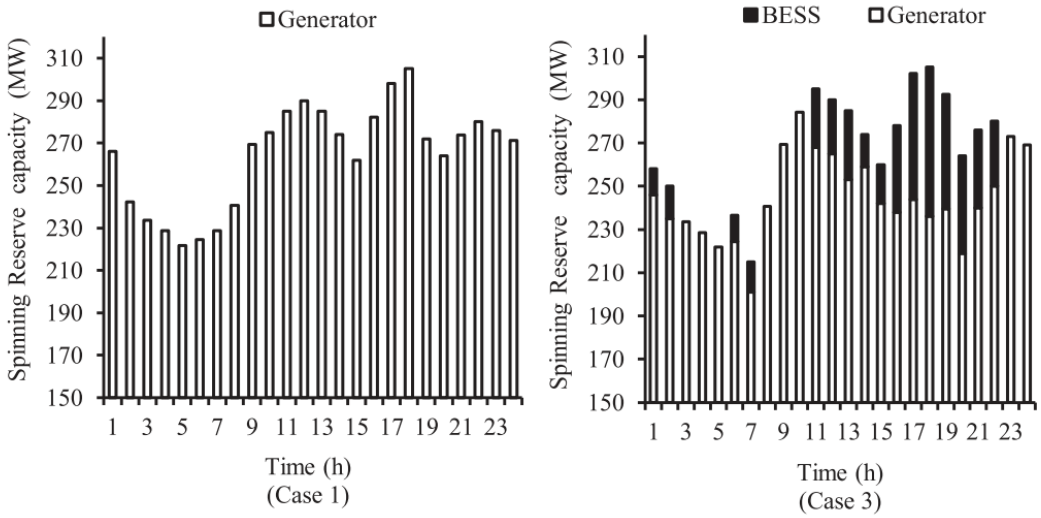

Figure 2-13: Spinning reserve contracted over 24 hours in Case 1 and Case 3. Adapted from Padmanabhan *et al.* [30].

Figure 2-13 shows the spinning reserve capacity between the two cases. By properly managing the charging and discharging rates, the batteries can provide ancillary services even during charging operations. It is possible to plan total dispatchable capacity available for contract by taking this into consideration. Padmanabhan *et al.*, aside from showing the benefit of energy sales with ancillary services, show the thoroughness of the cost of maintaining batteries and the importance of considering DOD and charging/discharging constraints, and how the reserve SoC fits into the equation. A weakness, however, is the narrow field of study for battery alone, rather than coupling with a generation method, in addition to a generic simulation tool that doesn't consider site location restraints.

3 Implementation and Research

3.1 Solar Irradiance Up-Sampling

For simplicity, the model of the solar panel itself is kept to a constant voltage supply, and a solar irradiance model is given to determine energy production on a minute-by-minute scale. The goal of the simulation is to keep the solar irradiance sampling at the same time scale as the simulation. Since site specific feeder data is being used, obtaining site specific solar irradiance data is also a priority. Data from the National Solar Radiation Database (NSRDB) [6] is sampled at 30 minute intervals, and must be up-sampled to the simulation sample rate.

The Markov model described in Section 2.2.1 is used to up-sample the data from 48 points per day to 1440 points per day (30 minute to 1 minute). Stochastic variability is added to the solar irradiance to mimic intermittent cloud cover that would be present in 1-minute data but is averaged out of 30-minute data. The benefit of the Markov chain is that the cloud cover is trained from previous data, making the future state only dependent on the present state.

3.1.1 Markov Chain

One-minute solar data is used to train the TPM by scaling the GHI versus clear-sky GHI as an indication of cloud cover (okta value). For the up-sampling, one-minute solar data should be used for the TPM. High resolution data is not available in the public domain and was cost prohibitive for this study. Therefore, only 1 year of data is used for a location within 150 miles of the facility site chosen. Okta values are generated from solar Global Horizontal Irradiance (GHI) data which is common among data sets. Clear-sky GHI is given as the maximum GHI possible at that time and day of the year at the specific location.

The transition probability matrix is built using the methods outlined in Section 2.2.1 with solar irradiance data from 2018. A plot of the TPM in Figure 3-1 confirms expectation of okta movement where the okta is likely to stay in its current state and less likely to change by large values, indicating an abrupt change in cloudiness, agreeing with literature presented in Section 2.2.1.

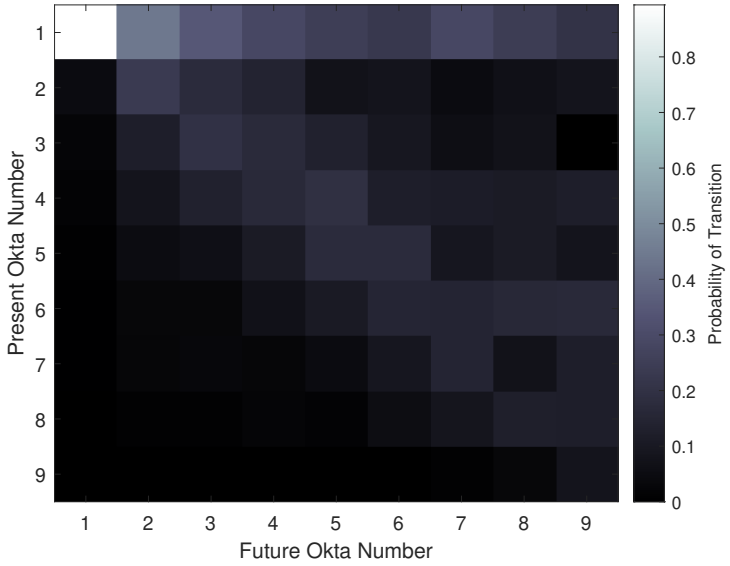

Figure 3-1: Transition Probability Matrix of the Markov Chain, 0-8 okta shown as 1-9.

It should be noted that there are fundamental differences in Figure 3-1 compared to Figure 2-3 since the data modeled is less than what is recommended [12, 13]. Once the transition probability matrix is formed using the one-minute data, local 30-minute data from other sites can be used for the simulations. This publicly accessible data from the NSRDB [6] contains both the variable GHI and the clear-sky GHI in 30 minute intervals. The Markov chain is run using the transition probability probability for each sample,

$$P = T \cdot X_0 \tag{7}$$

where T is the transition probability matrix, X_0 is the current okta value as an array, and P is the probability of the okta value X_1 takes. A random number generator is used to weight the probabilities and choose the okta value of X_1. The data is tested for a specific day from available data. The original data is shown in Figure 3-2. The resultant up-sampled data using a Markov chain is shown in Figure 3-3.

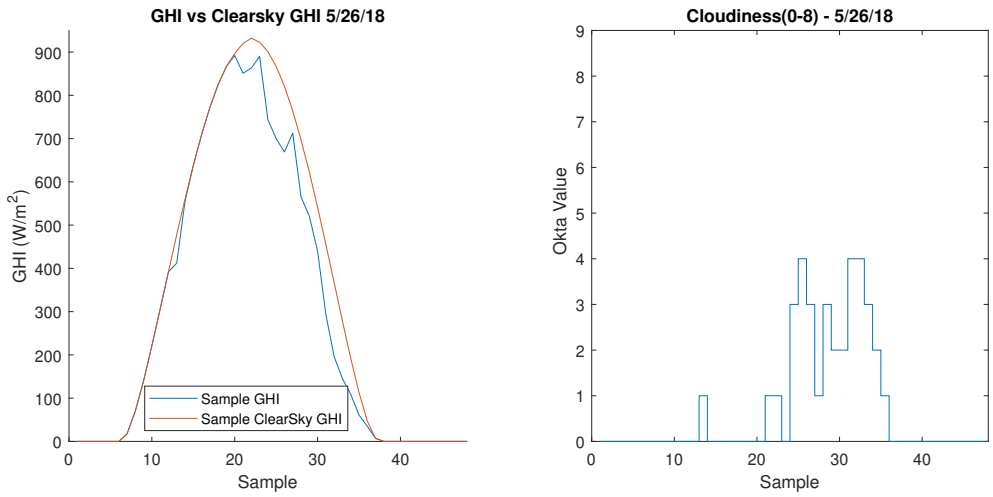

Figure 3-2: Native 30-minute GHI data chosen for one day, May, 26, 2018 with okta value.

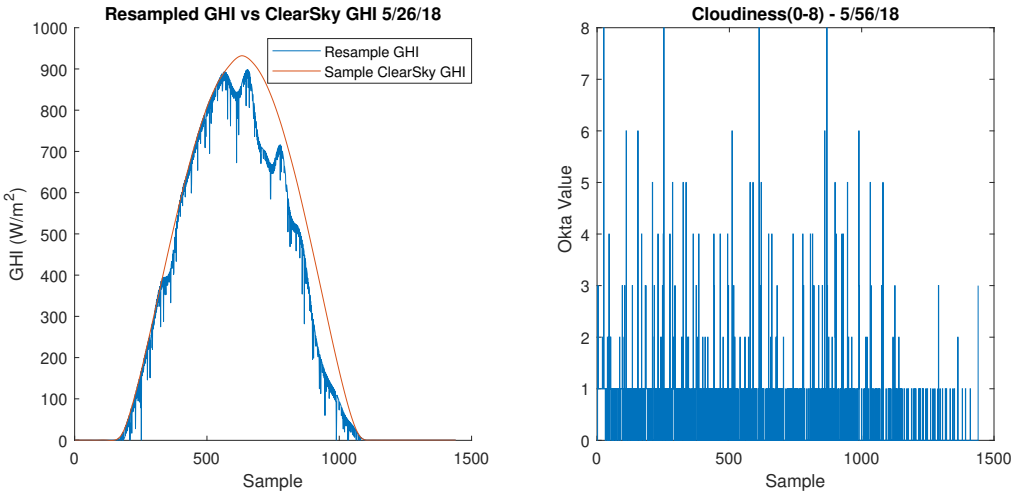

Figure 3-3: Up-sampled GHI using Markov chain with okta value.

After initial runs of the Markov chain to model variation, it is noticed that care must be taken that the one-minute samples do not become erratic due to rapid changes in the okta value based on the Markov chain. The solution is to change the process such that multiple okta value changes over a given interval must be triggered from the Markov chain before a change in okta value is recognized. The sample is re-run with a 5-minute interval for okta changes and is applied to smooth the high-frequency okta values. A different day is tested with the updated Markov chain application giving the results in Figure 3-4. This shows that the up-sampling accurately adds intermittent cloud cover representative of high-frequency changes in cloud cover.

(a)

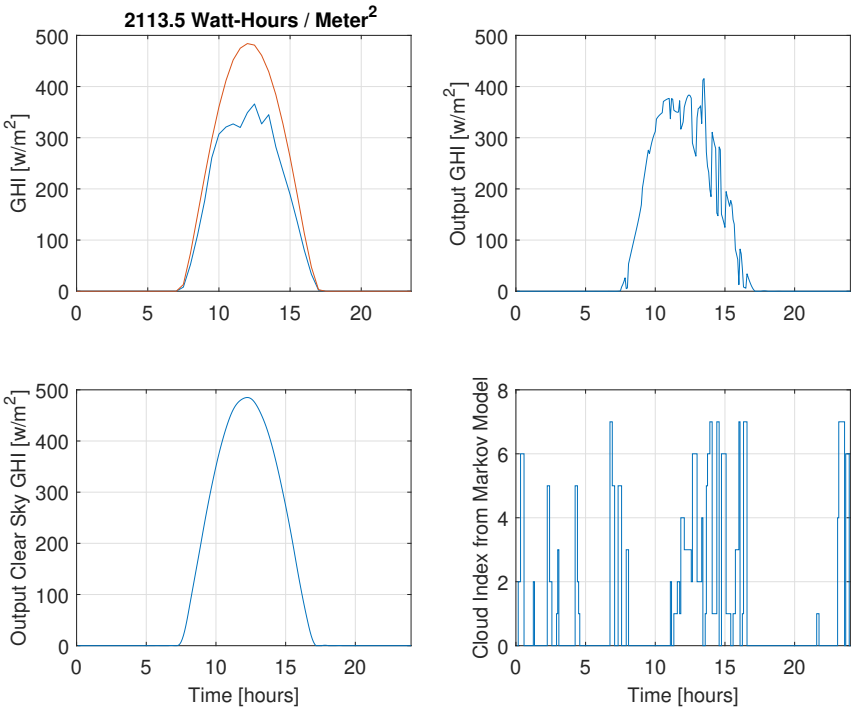

(b)

Figure 3-4: (a) Up-sampled GHI using Markov chain and short-interval averaging. (b) Detailed results of Markov chain application with okta value.

3.2 Validation of Simulation Results

Validation was performed on the PSCG simulation comparing the simulation's results to Synergi Electric's results when fed the simulated real and reactive power with corresponding load. For every simulation, results are given for voltage at the substation, KW into grid, KVAR into grid, total losses, and load tap change position.

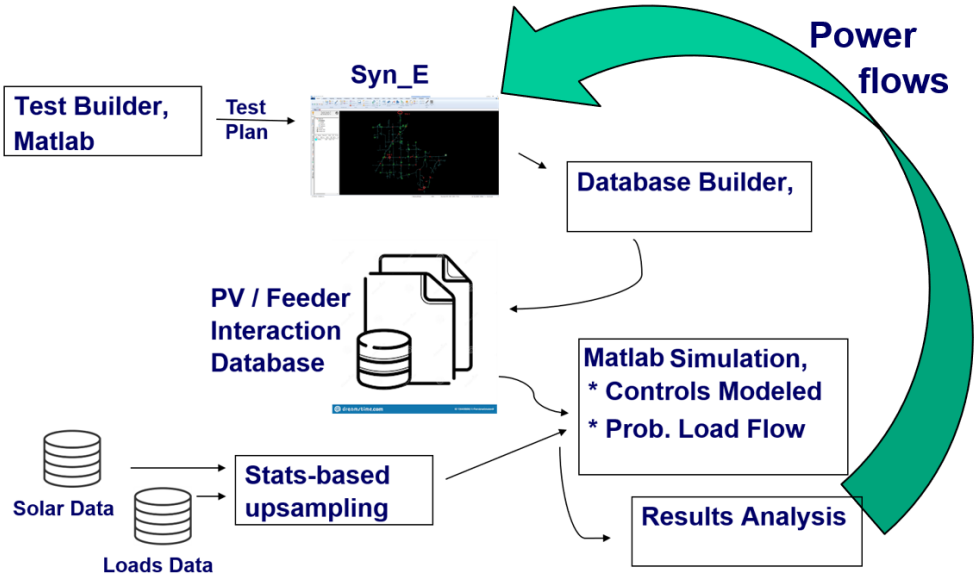

Figure 3-5: Validation of PSCG simulation with Synergi Electric integration. Adapted from Chatradi et al. [2]

The validation process is visualized in Figure 3-5 with the PSCG Simulation flow from Figure 2-1. First, an input file for Synergi Electric is built using the PSCG simulation outputs as the base of the model. Synergi Electric's Time Series Analysis is used with the load, KW into grid, and KVAR into grid to produce the same data that is collected in the PSCG simulation during the database building process. In theory, if the simulation is accurate, the resultant voltage at the site feeder from the simulation should match Synergi Electric's result. For the case of validation, voltage is normalized to 120 Volts.

The first pass of validation showed an RMS voltage difference of 0.76V, shown in Figures 3-6 and 3-7, which pointed to a problem in the simulation.

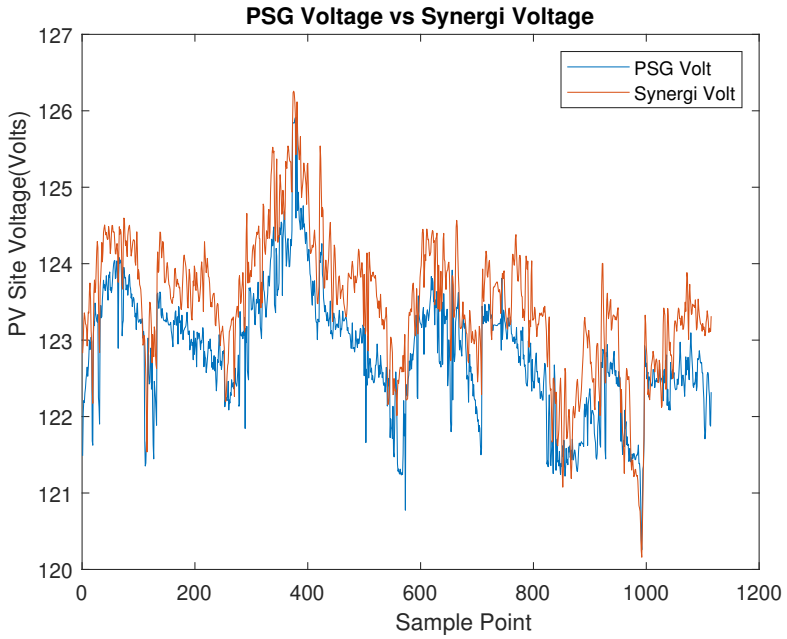

Figure 3-6: Validation of PSCG simulation voltage compared to Synergi Electric voltage.

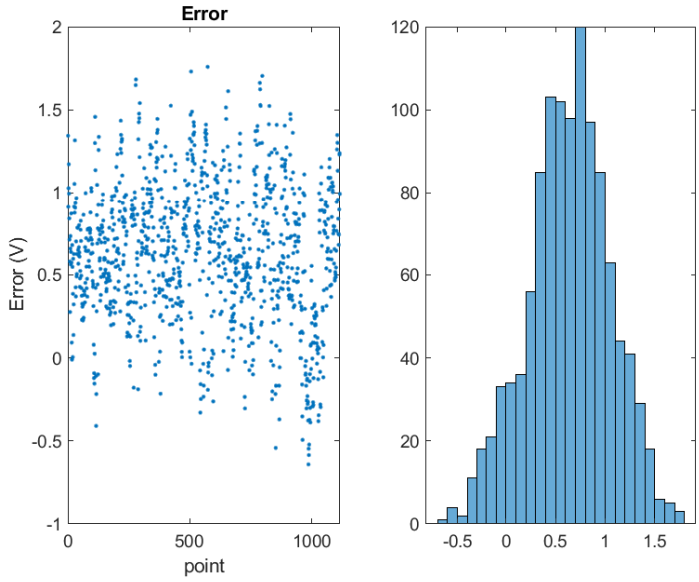

Figure 3-7: Scatter plot and histogram of PSCG voltage and Synergi Electric voltage error.

As seen in the figures, the error looked like a consistent offset between the two results. When looking at the load tap changer of the simulation, shown in Figure 3-8, it was evident this was where the problem resided. The Synergi Electric simulation showed a single change in the load tap changer while the simulation

produced many changes in the LTC's position. From a practical standpoint, this is clearly not correct since normal load tap changer movements are reduced by hysteresis.

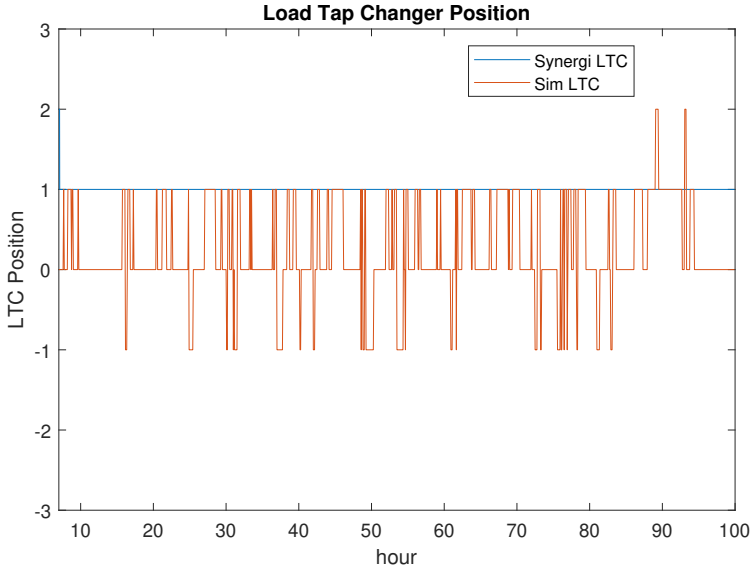

Figure 3-8: PSCG load tap changer compared to Synergi Electric load tap changer.

Since a real load tap changer is a mechanical device, a model needed to be built reflecting Synergi Electric's load tap changer in order to accurately predict the position of the simulation's load tap changer. This error is unique to the case of this simulation. Since real feeder data and responses are being pulled from a separate simulation (Synergi Electric), the PSCG simulation must accurately predict the non-linear LTC component of the Synergi Electric simulation.

3.2.1 Load Tap Changer Modeling

Examining Synergi Electric's LTC model and papers' findings, a different approach was taken for the LTC model rather than using the load tap changer's physical model. This was done since the simulation should be site specific rather than narrowed to a single LTC in Synergi Electric's feeder system. The Synergi Electric documentation of the LTC operation within the model allows an approximation to be made using available data. The database building routine of PSCG was adapted to sweep across a wider range of input power (real and reactive) without adjusting load to cause the LTC to change rapidly. This gives multiple points of variation for the LTC to build a model that will accurately predict the LTC position during future simulations. The data is first cleaned up by using points only when the load tap changer is changing taps to identify the voltage direction. If the voltage is dropping due to a decrease in input KW or increase of KVAR, the LTC will eventually shift one tap higher to decrease the turns ratio on the secondary winding,

increasing the voltage. For the model, a linear equation is used for parameter estimation in the form

$$\hat{S} = \phi\theta \tag{8}$$

where ϕ is a regressor vector using Input KW, Input KVAR, Load, and Direction. The square of each parameter as well as cross-coupling is added to the vector to improve accuracy. This gives the equation for the LTC model as

$$\begin{aligned}\widehat{LTC} &= a + b \cdot \text{KW} + c \cdot \text{KVAR}, + d \cdot \text{Load} + e \cdot \text{Direction} + \\ &f \cdot \text{KW}^2 + g \cdot \text{KVAR}^2 + h \cdot \text{Load}^2 + \\ &i \cdot \text{KW} \cdot \text{KVAR} + j \cdot \text{KW} \cdot \text{Load} + k \cdot \text{KVAR} \cdot \text{Load}\end{aligned} \tag{9}$$

Table 4 gives the corresponding θ values from the parameter estimation:

Table 4: LTC Parameter Estimation coefficients.

Parameter	**Regressor**	**Value**
a	1	-1.26071
b	KW	0.000241
c	KVAR	0.000642
d	Load	3.423068
e	Direction	-0.925829
f	KW^2	1.198008 $\cdot 10^-8$
g	KVAR^2	5.831782 $\cdot 10^-9$
h	Load^2	0.194826
i	KW·KVAR	-1.201218 $\cdot 10^-8$
j	KW·Load	6.344380 $\cdot 10^-5$
k	KVAR·Load	4.107258 $\cdot 10^-6$

The parameter estimation shows a strong correlation of the LTC to the current load and direction with a smaller correlation from KW and KVAR. The LTC is then tested against the source data giving an RMSE of 0.2759. The results in Figure 3-9, with a portion zoomed in for Figure 3-10, show minor variations from Synergi Electric's load tap changer from the PSCG simulation.

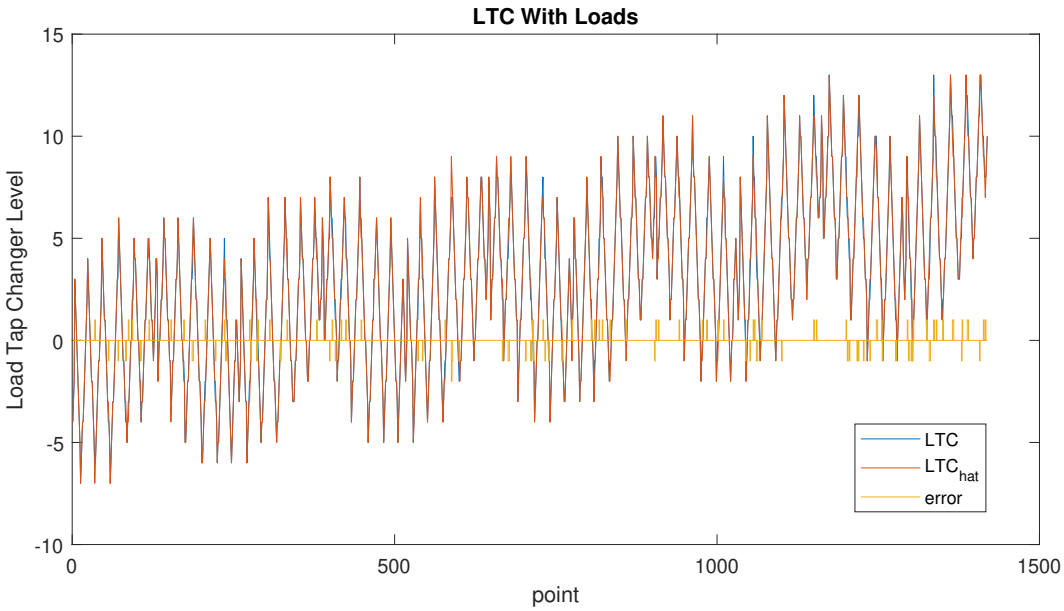

Figure 3-9: Validation results of adapted modeling LTC, Synergi Electric in blue, PSCG simulation in orange, error in yellow.

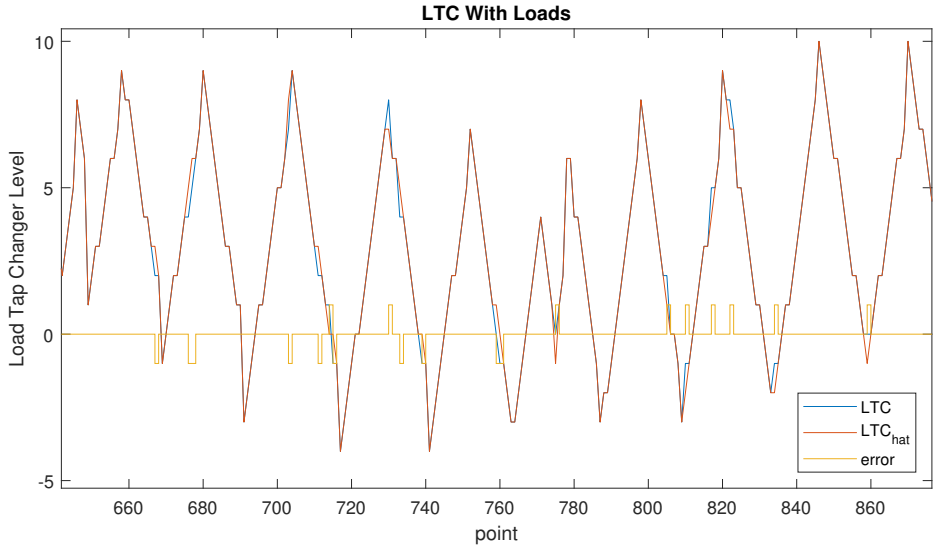

Figure 3-10: Zoomed - Validation results of adapted modeling LTC, Synergi Electric in blue, PSCG simulation in orange, error in yellow.

3.2.2 Validation of Simulation with Modeled LTC

Once the modeling for the load tap changer is complete, the validation routine is run again with the same data. The LTC model accurately predicted the LTC position during the run of the simulation as shown

in Figure 3-11. This validation result shows several important factors of the overall simulation. First, the correct modeling of the LTC tracks the Synergi Electric voltage output much more closely than previously and lowered the RMSE from the prior 0.76V to 0.11V as shown in Figures 3-12 and 3-13.

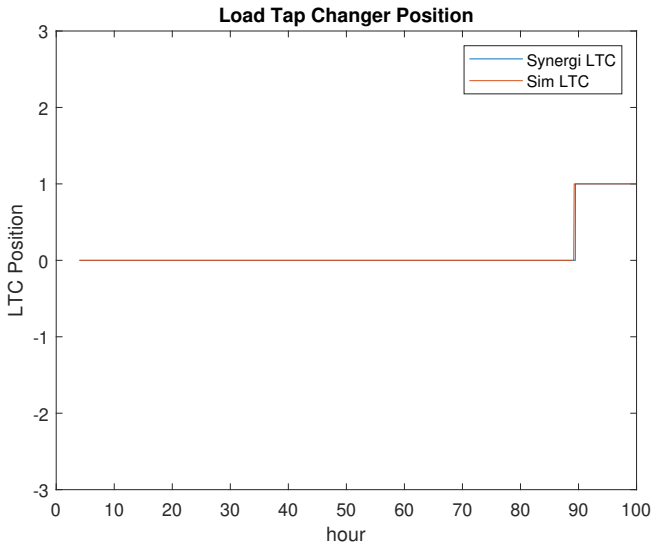

Figure 3-11: Validation PSCG simulation set over 100 hours with modeled LTC, PSCG simulation compared to Synergi Electric.

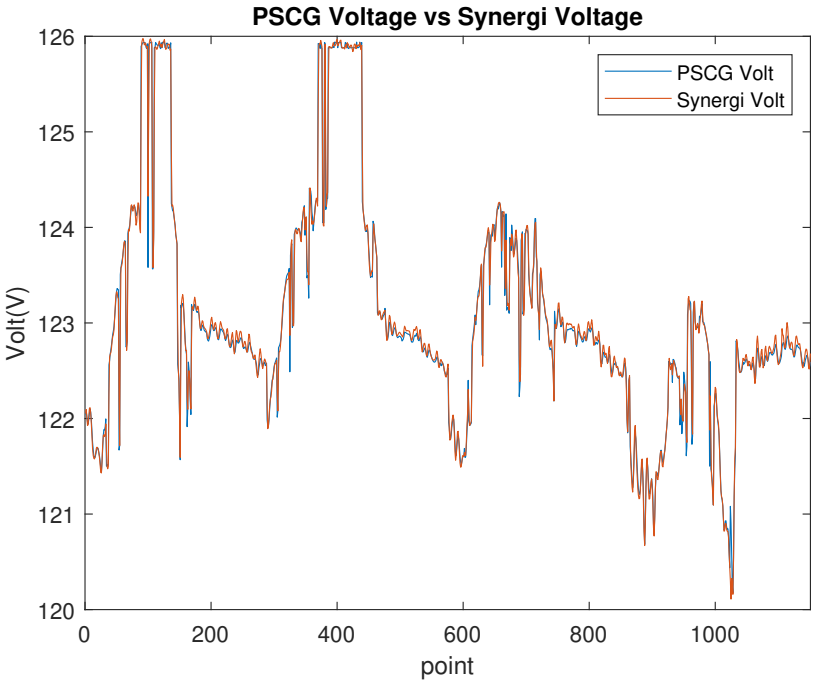

Figure 3-12: Validation of PSCG voltage compared to Synergi Electric voltage with modeled LTC.

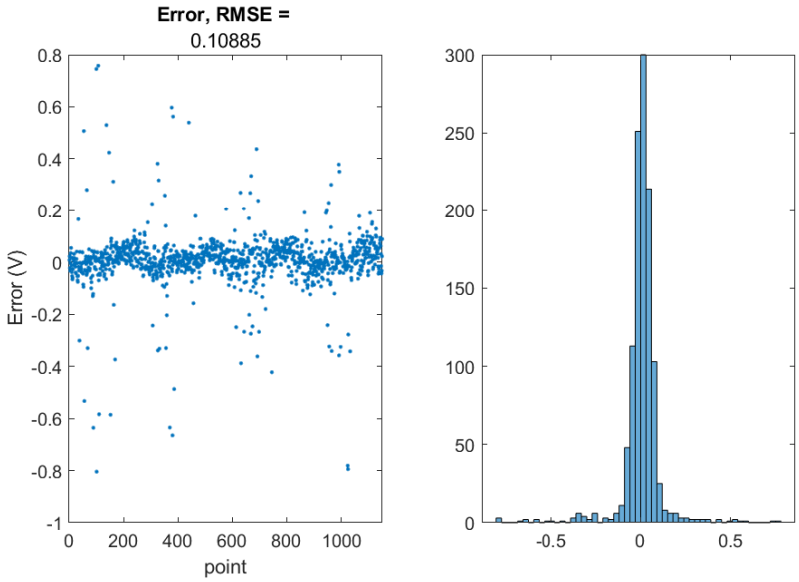

Figure 3-13: Scatter plot and histogram validation of PSCG voltage and Synergi Electric voltage error.

A second aspect of the correct simulation to consider is the limited number changes in load tap changer position. The simulation's controller is able to keep the voltage near the nominal range enough that LTC changes once within a 100 hour period. Since the LTC produces arcing due to high current with every tap change, it must be maintained after a specified number of tap changes. It is assumed the total tap changes can vary but multiple sources pointed to 75,000 tap changes [15, 16] as a metric. At this rate, the LTC would need less frequent maintenance with properly controlled voltage.

3.3 Dispatchable Capacity Provision

The analysis tool produced as contribution for this thesis focuses on the potential for dispatchable capacity via a capacity contract. Dispatchable capacity as an ancillary service can provide a source of revenue for PV and battery facilities aside from arbitrage. Since the dispatchable capacity is rarely called upon [22], the passive income from a capacity contract is also a way to lessen degradation of the battery in comparison to arbitrage. The battery, more often than not, will sit with a reserve state of charge through the contract interval unless called upon to dispatch. The process can be summed up:

- Consider a contract for spinning reserve, rapid η MW boost in power, upon dispatch
- Provision over 6-hour contract interval from 6pm to midnight
- One-hour dispatch duration

- Estimate maximum dispatchable capacity

The time of 6pm-midnight is chosen and works well for solar sites with batteries. The batteries will charge via PV during the day while control laws manage a state of charge reserve to enhance the maximum dispatchable capacity. At this point, the sun has gone down and the site can choose to discharge any extra energy into the grid when needed while still maintaining a minimum charge for dispatchable capacity. The two-fold benefit comes from relying on the control laws to ensure enough energy is present in the battery by nightfall and capitalizing on the higher energy sale price during the high load times.

The potential for dispatchable capacity is separated into multiple sections. First, site limits are calculated and an overall minimum dispatchable capacity is obtained from the result. This would be a worst-case scenario for dispatchable capacity as it takes the worst minute of the entire year. A better consideration of the limits is done in two ways: 1) by taking the minimum of each month and averaging all 12 months; and 2) by using a statistical approach of fitting a Weibull distribution determining the dispatchable capacity values corresponding to 99.99% and 99.9999% confidence of being able to provide power at that value. These give a better calculation of the 1:1,000 and 1:1,000,000 chance of failing to fulfill a capacity contract. The three limits considered are as follows:

1. Grid connection limit, [MW], determined by MVA and voltage constraints
2. Battery power electronics limit, [MW], [MVAR], and [MVA]
3. Stored energy in the battery, [MWh]

Limit 1 is determined solely by the PV and storage site location. This is made possible by Synergi Electric's modeling tool giving feeder response to site MW and MVAR flows. For the simulation, a specific site is chosen with a grid connection power limit of 8MW. The grid connection ends up becoming a primary limiting factor as the size of the facility grows.

Limit 2 is determined by the battery power electronics and requires a non-linear approximation due to the relationship of MW and MVAR to provide power into the grid. The ability to control voltage is considered from both the MW (increasing voltage) and MVAR (decreasing voltage) viewpoint. There must be enough headroom in the battery power electronics to provide the required power to the grid connection.

If limits 1 and 2 are satisfied in the facility's sizing and grid connection, then limit 3 is the logical conclusion to the potential for dispatchable capacity—that is the energy stored in the battery. For this scenario, the capacity contract is kept to a 1 hour duration to satisfy MISO's minimum duration requirement [30].

3.3.1 Limit 1 - Grid Connection

The limit of the grid connection relies on Synergi Electric's grid feeder model. Site 1 is used throughout this study, rated at 8MVA (8206KVA exactly). Site parameters are shown in Table 5.

Table 5: Site study parameters with feeder parameters.

	Miles From Substation	**Connection (AWG/MCM)**	**Impedance**	**Max MVA**
Site 1	16.1	#2 ACSR	$Z\_0 = 14.3 + j37.3$	8.208
Site 2	8	#2 ACSR	$Z\_0 = 11.5 + j21.5$	8.208
Site 3	7.9	336 ACSR	$Z\_0 = 5.4 + j18.6$	20.736

Feeder: V_{p-p} 24.9kV, 2.6/5.3MW mean/peak

#2 AWG ACSR - 190/260A mean/peak, 336MCM ACSR - 520/730A mean/peak

Additionally, the site is relatively distant from the substation, resulting in a voltage imposed limit of 2.0 to 4.8MW, depending on the current load, assuming an LTC tap of zero, and no use of VARs to manage the voltage. Limit 1 is applied as a way to constantly monitor the power into the grid as to not exceed the voltage or MVA limit of the feeder. The limit is obtained by the real and reactive power currently at the site, P and Q respectively, and the estimated maximum voltage on the feeder as a combination of P, Q, and S, the MVA boundary of the system. The feeder database is used to iteratively estimate the maximum real and reactive power that can be injected into the grid, given as $\hat{P}$ and $\hat{Q}$. Limit 1 is the difference of the maximum possible real power ($\hat{P}$) less the current input real power into the grid

$$\text{Limit}_1 = \hat{P}_{max} - MW_{input} \tag{10}$$

3.3.2 Limit 2 - Battery Power Electronics

The limit of the battery power electronics is calculated based on the real and reactive power required to reach the maximum voltage allowable, in this case just under 126V. This is done at each simulation step. The limit calculation utilizes an interpolation routine built in to the PSCG simulation to predict the voltage at a given battery MW and MVAR input. The battery MW and MVAR constraints are based on the maximum of the battery power electronics minus the current usage. For example, if the current simulation run is set up to have 4MW of battery power and the battery is discharging 300kW of power, then the maximum battery input MW is determined to be 3.7MW of power. This method is important as it considers, for each step of the simulation, what is the real feasible capacity of the power electronics to delivery power into the grid.

Since the MVAR can counteract the rise in voltage from MW input, MVAR is also considered with a usable constraint. Figure 3-14 shows the visualized representation of the battery power electronic limits in KW and KVAR. The red X marks the current battery power KW and KVAR usage. In this case there is approximately 700kW of generating real power and no KVAR present. The dashed green line around the corners are the total power in KVA that the system can produce and, since the relationship is quadratic, it is not a straight line. This is what makes the calculation of battery power electronics more complicated than simply taking the maximum real power constraint.

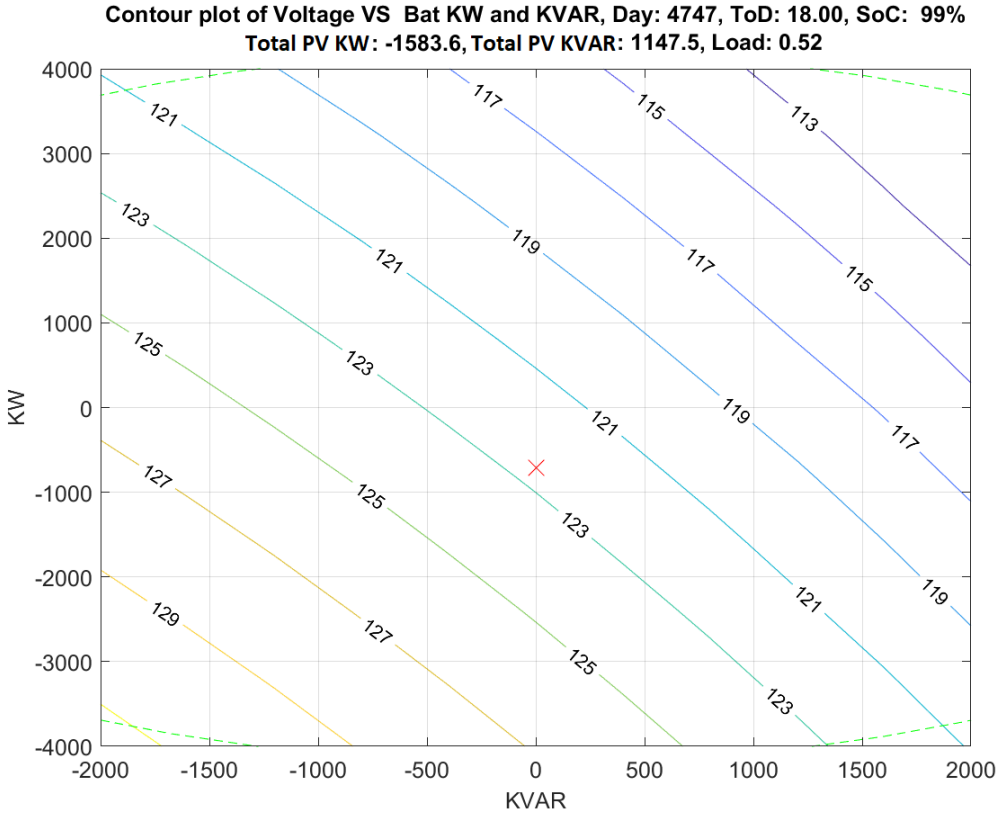

Figure 3-14: Battery power constraint of limit 2 visualized by current KW and KVAR with voltage constraint.

The first step in calculating the limit is to find the edge of the green dashed line, given as the bounding constraint of the KW and KVAR of the power electronics. In the plot, KW is considered negative for generating, giving the area of interest in the lower right corner. The first, shown in Figure 3-15 at the point of the circle, is the KVAR constraint at the maximum bound KW. The second, at the point of the square, is the KW constraint at the maximum bound KVAR.

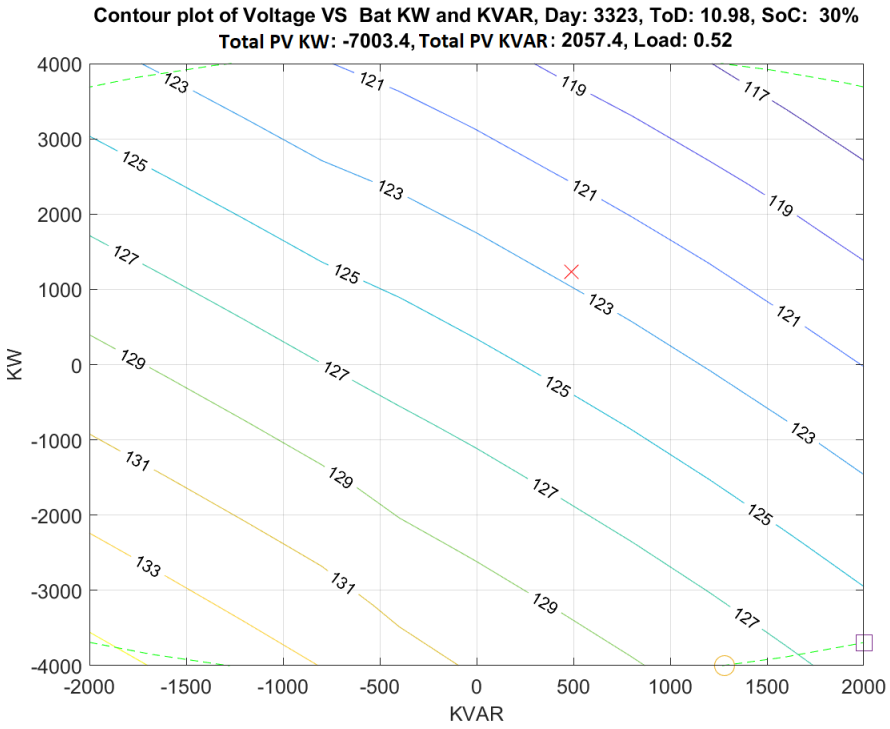

Figure 3-15: Battery power constraint of limit 2 visualized by bound KW and bound KVAR (square and circle) with voltage constraint.

To calculate the limit, the voltage is calculated with the current load and the KW and KVAR constraints. The maximum and minimum voltages, shown as a circle and square respectively, are visualized in Figure in 3-15. If the maximum voltage falls on the KVAR axis, such as in Figure 3-14, then the limit is simply the maximum KW power constraint boundary and there is an excess of KVAR available to achieve the maximum voltage. If the maximum voltage falls on the KW axis, then the maximum KW power is the KW constraint at the maximum bound KVAR, shown in Figure 3-15 as approximately 3200KW, just above the square point along the KW axis.

If the maximum voltage falls on neither the KW nor KVAR axis and within the green dashed line, such as in Figure 3-16, then the power electronics limit must lie somewhere between the two points on the dashed green line. The range of voltage is scaled from 0 to 1, shown as ϕ, with 0 being the square and 1 being the circle point. This is the high and low range of the voltage at the edge of the KW and KVAR boundary. A mid-point of 0.5 is chosen and fit to a quadratic to determine the point at which the maximum voltage exists

within the KW and KVAR constraints. This is given by

$$\begin{aligned} \phi &= \begin{bmatrix} 0 & 0.5 & 1 \end{bmatrix} \\ \bar{y} &= \begin{bmatrix} V_{\circ} & V_{mid} & V_{\square} \end{bmatrix} \\ &\text{Taking the pseudo-inverse of } \phi \text{ and } \bar{y} \\ \hat{\theta} &= (\phi' \cdot \phi)\phi' \cdot \bar{y} \end{aligned} \tag{11}$$

Solving for the quadratic equation to obtain ϕ at V_{max} where

$$\begin{aligned} \phi_{V_{max}} &= \frac{-\theta_2 \pm \sqrt{\theta_2^2 - 4\theta_1\theta_3}}{2\theta_1} \\ &\text{for} \\ \phi > 0 \quad &\text{and} \quad \phi < 1 \end{aligned} \tag{12}$$

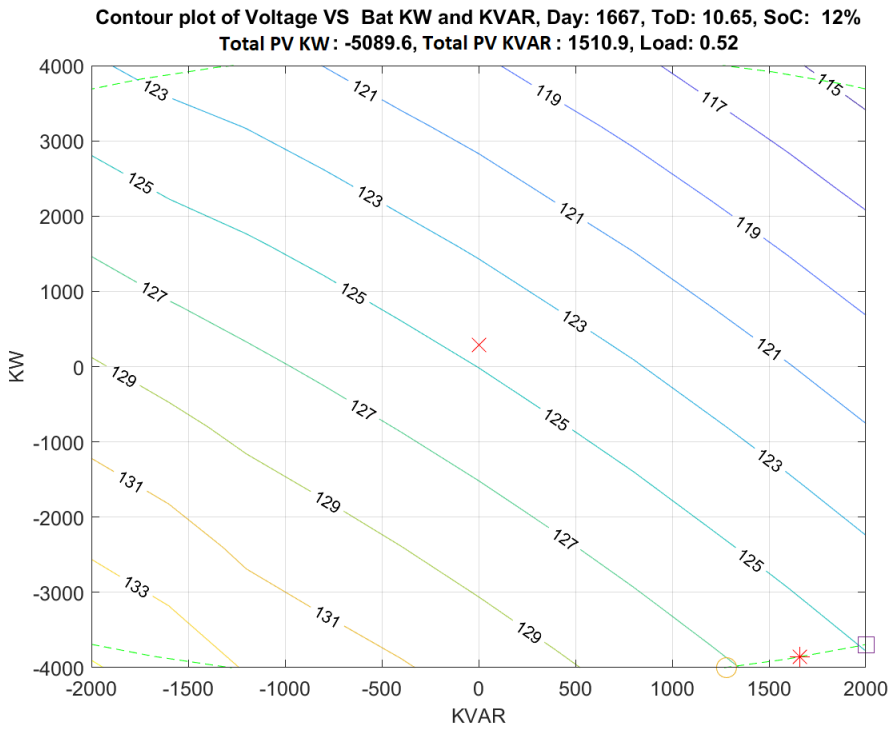

Figure 3-16: Battery power constraint of limit 2, KW and KVAR constraint at maximum voltage.

Once ϕ is calculated for V_{max} within the KW and KVAR constraints, shown in Figure 3-16 as the red asterisk, the interpolation routine is run with the given load, KW and KVAR from ϕ to confirm the value

obtained is accurate to the true V_{max}. This gives the second limit of the dispatchable capacity as the limit of the battery power electronics to deliver power into the grid.

3.3.3 Limit 3 - Stored Battery Energy

The third limit of the dispatchable capacity is the stored energy in the battery over the contract duration. The stored battery energy is directly related to the control law in effect during the simulation. This is a pivotal portion of the potential for dispatchable capacity evaluation as it creates a trade off between the dispatchable capacity at any given time to fulfill an ancillary services contract and the capability to inject energy into the grid for a separate wholesale energy revenue. For initial simulations, the reserve state of charge in the battery is kept at 10% to simplify observation of facility sizing differences on how limits are affected. Later simulations compare multiple reserve state of charge percentages to consider the optimal state of charge for a given facility configuration.

In calculating the battery energy storage limit, the selected dispatch duration affects the battery's ability to deliver power. The dispatch duration chosen is taken into consideration with the discharge rate of the battery and the energy in the battery. In the current study, the dispatch duration is set to 1 hour. The limit is determined by looking forward in time over the contract duration and taking the minimum available energy in the battery during the dispatch duration. In Equation (13), X is the minimum charge of the battery during the contract duration, $R(t)$ is the current charge in the battery for each sample time, t_0 is the start of the dispatch duration, and t_1 is the end of the dispatch duration.

$$X = \min\{R(t), t_0 < t < t_1\} \tag{13}$$

This equation is carried out in a loop for all of the 525,000 time samples of the simulation (1 minute sampling for 1 year). It is then trimmed to the selected contract duration of 6pm to midnight. Both the current and future battery energy storage is known for the length of the contract duration, ensuring that the chosen dispatch duration can be fulfilled over the entire contract duration.

3.3.4 Limit Review by Facility Sizing

There are 3 main facility parameters inspected first. That is:

1. PV Sizing [MW]
2. Battery Power Electronics Sizing [MW, MVA]
3. Battery Duration [hours]

For each case, one parameter is locked and the other two are left as variable and the affect of the variability on each limit is examined. Knowing how each facility parameter can affect each limit can help to identify where the bottleneck is in a given system. Each parameter is evaluated in a range based on a sizing of $\frac{1}{4}$, $\frac{1}{2}$, 1, and 2 times related to either the site or facility parameter. The limits are plotted as the overall combined minimum while also defining which limit is active during each month, showing important seasonal differences apparent in facility sizing.

Comparing PV Sizing

The first parameter examined is PV sizing. The sizing is in relation to the site max MVA at the feeder of 8MVA, so the PV sizes considered are 2MW, 4MW, 8MW, and 16MW. As a first example, a relatively low battery power of 4MW is examined with a duration of 4 hours, or 16MWh total.

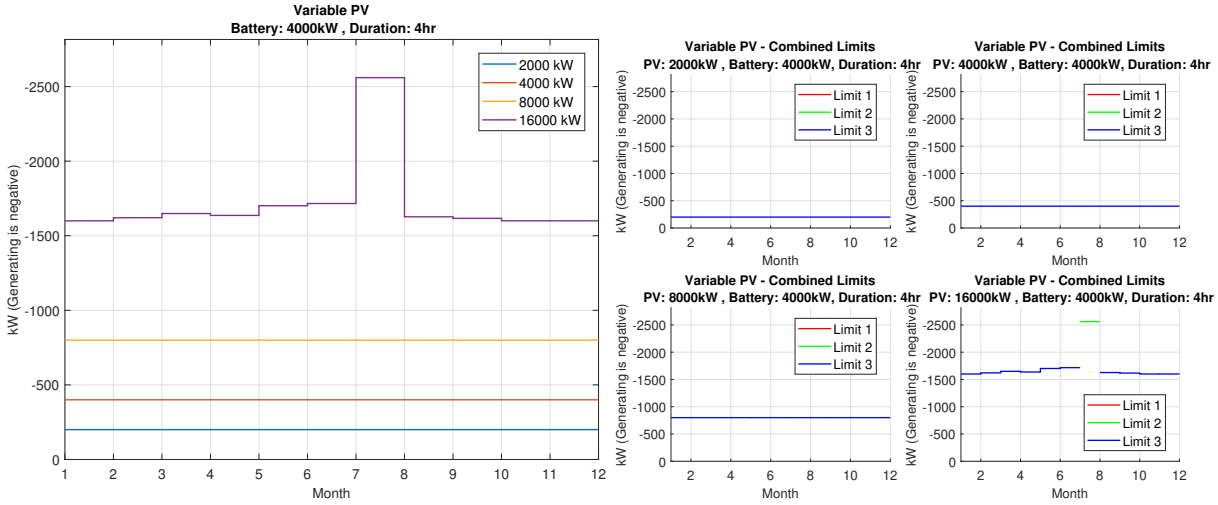

(a) (b)

Figure 3-17: (a) 4MW Battery, Variable PV sizing (b) Overall limit visualized by active limit

Figure 3-17a and 3-17b show the overall minimum of dispatchable capacity for variable PV sizing. With the reserve state of charge at only 10%, the overall limit of the dispatchable capacity becomes limit 3 (the battery energy storage), for 2MW, 4MW, and 8MW PV. This is mostly due to control law as the system is sending the most power into the grid during the day and only leaving a small portion in the battery once the start of the dispatch duration is reached. As the PV size gets larger, the 10% minimum state of charge is less of a concern as excess power is diverted into the battery to avoid curtailment. Once the PV is sized at 16MW, limit 2 (the battery power electronics) is active during July (*cf.* Figure 3-17a,b) due to the battery being fully charged by excess PV generation. It is important to note the increased production during summer months when the irradiance is highest.

Examining a case with greater battery power gives the case where the site location (limit 1) becomes the limiting factor. Figure 3-18 shows a facility with 4x battery power and energy as the previous (battery duration is 4 hours in both cases). In this case the control law is keeping the reserve SoC in the battery lower with lower PV sizing as in the previous case. However, the largest PV size proves to be a deficit as it causes the grid to be saturated by the high PV (*cf.* Figure 3-18b, the 16MW case, where dispatchable capacity crashes during the summer months, due to limit 1). During summer months the power generated and stored in the battery is then discharged at a high rate to prevent curtailment from the PV. For the case of a contract for dispatchable capacity, it is imperative to be able to account for the time in which the facility is unable to input the power requested due to limits of the grid connection.

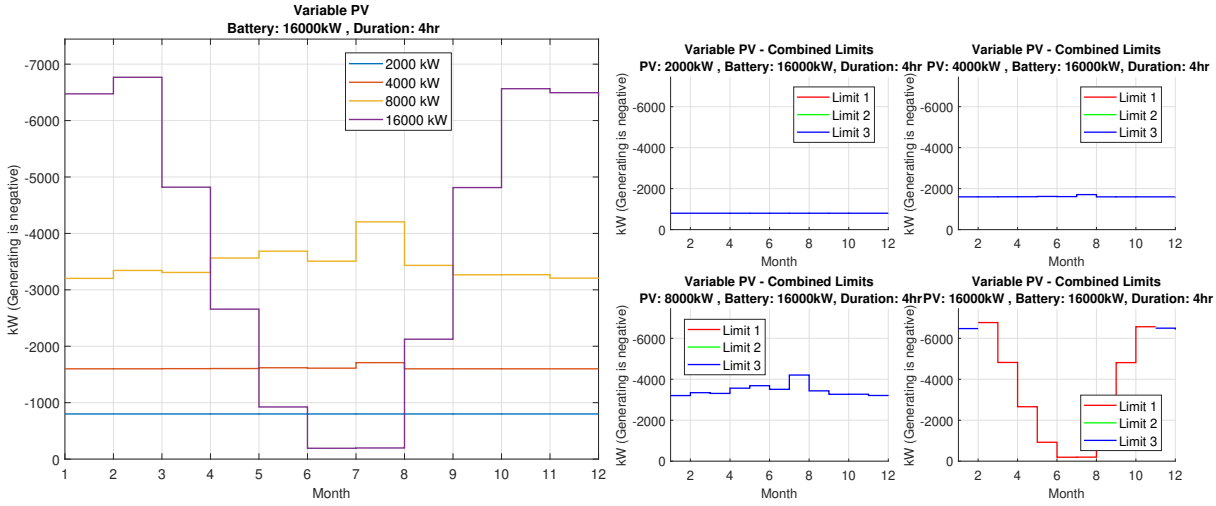

(a) (b)

Figure 3-18: (a) 16MW Battery, Variable PV sizing. (b) PV visualized by active limit.

Comparing Battery Duration

Battery Duration is compared at 1, 2, 4, and 8 hours. This is then multiplied by the battery power to appropriately size the battery energy storage. As the duration of the battery increases, the potential to store more energy in the battery also increases. In this case, the size of the PV can become a limiting factor. Figure 3-19 shows the effect of varying duration at 8MW PV and 8MW battery. As the duration and, consequently, the total battery energy storage increases, dispatchable capacity increases with the battery energy storage being the limiting factor, except for the longest battery duration of 8 hours. Under the control law, the battery discharges power back into the grid to maintain the potential to charge and avoid curtailment of the PV. The 8MW PV, 8MW battery, and 8 hour duration ends up being a relatively good candidate for dispatchable capacity since at the 8MVA grid connection limit, dispatchable capacity rests at approximately a 6MW average with only a slight decrease in the summer due to the grid connection.

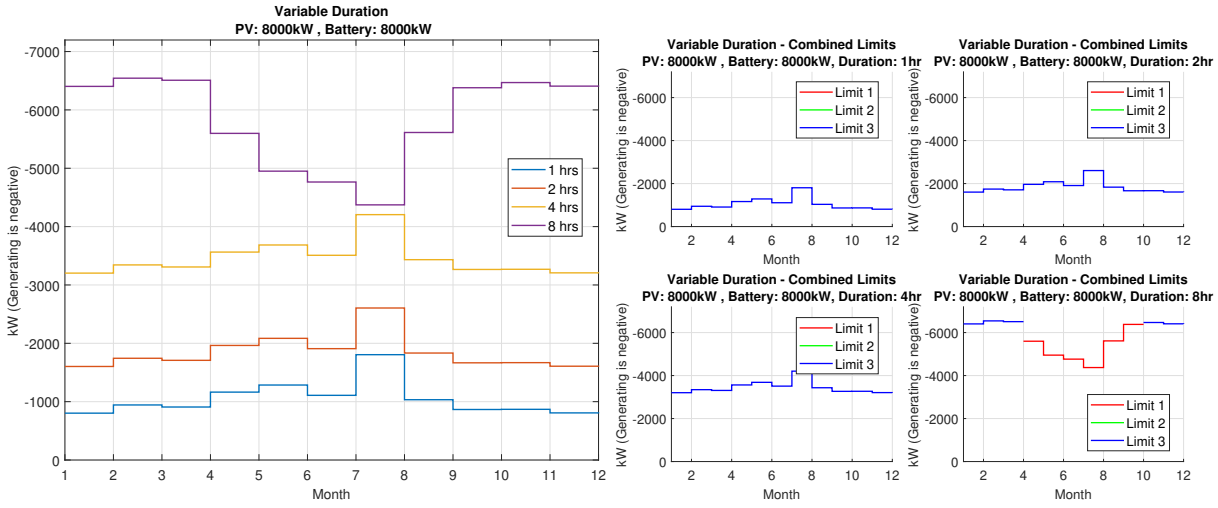

(a) (b)

Figure 3-19: (a) 8MW PV, 8MW Battery, Variable Duration. (b) Duration visualized by active limit.

Comparing the same durations and a larger PV facility of 16MW shows a vastly different outcome, as shown in Figure 3-20. The oversized PV facility ends up becoming a detriment to the dispatchable capacity once again. At higher energy capacity, the system ends up sending a considerable amount of power into the grid, effectively making the potential dispatchable capacity near zero during summer months due to saturating the grid connection. The oversized PV will try to send power into the grid or into the battery to avoid curtailment. Even at a larger battery energy capacity of 64MWh, the PV facility, which is 2x larger than the grid connection, ends up with a lower dispatchable capacity as the power generation and battery energy storage are greater than the grid connection's capability to fully receive the stored energy.

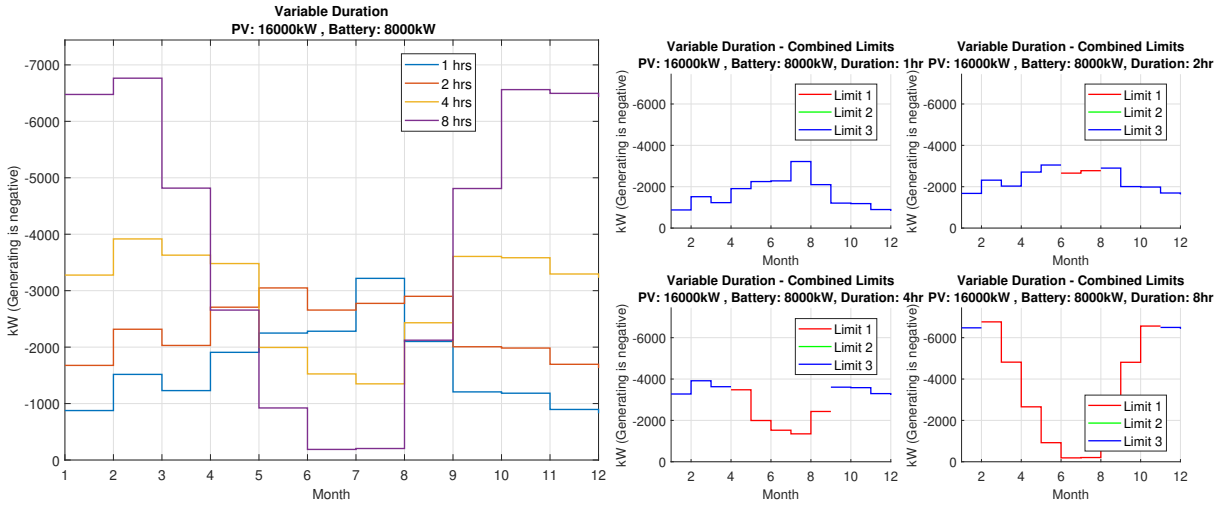

(a) (b)

Figure 3-20: (a) 16MW PV, 8MW Battery, Variable Duration. (b) Duration visualized by active limit.

It can also be seen in Figure 3-20 that while the 8 hour duration shows a non-ideal dispatchable capacity case, the cases of 1, 2, and 4 hour durations actually give a near-equal potential for dispatchable capacity as the smaller 4MW PV. In the case of the 4 hour duration, there is lower dispatchable capacity during the summer months of high irradiance. The over-sized PV agrees with the PV sizing in Figure 3-18 where the overall energy production with grid connection limits effectiveness of dispatchable capacity due to the inability to discharge energy back into the grid rapidly enough. This glance at the effect of duration on dispatchable capacity shows that the duration can greatly impact the dispatchable capacity due to increased energy storage.

Comparing Battery Power Electronics Size

Battery power electronics are sized based on the associated PV sizing following the same trend of $\frac{1}{4}$, $\frac{1}{2}$, 1x, and 2x of the PV sizing. This gives a view of how the battery power, compared to the PV sizing, can affect the potential for dispatchable capacity. This view also gives better insight into the grid connection in relation to both the PV and battery power. Since the relationship between the PV and battery duration are kept constant, it is easier to see the point at which the grid connection begins to saturate. Starting with a look at a relatively small PV sizing at a quarter of the grid connection limit, Figure 3-21 shows the potential for dispatchable capacity increasing with the battery power size from 0.5 to 4.0MW.

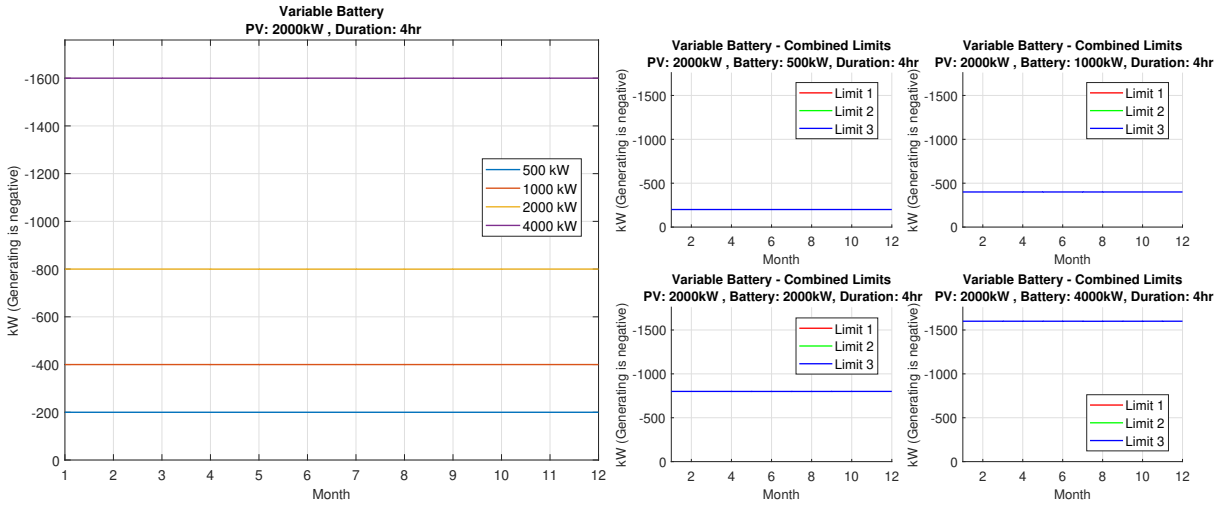

(a) (b)

Figure 3-21: (a) 2MW PV, 4hr duration, variable battery power. (b) Battery visualized by active limit.

Considering Figure 3-22 with 8 hour duration, as the battery power grows, the limit begins to change from battery energy (limit 3) to battery power (limit 2), eventually saturating the grid (limit 1). With the variable battery power, the duration then scales the size of the battery—in this case 8MWh to 64MWh. This method specifically gives insight into controlling cost as well. The battery power electronics are considerably cheaper than PV and battery duration, allowing an optimal configuration to be reached that gives the most dispatchable capacity based on PV and battery energy. In this case, a 4MW PV and 8MW battery at 8 hour duration performs better than the case in Figure 3-19 with greater dispatchable capacity during the summer months.

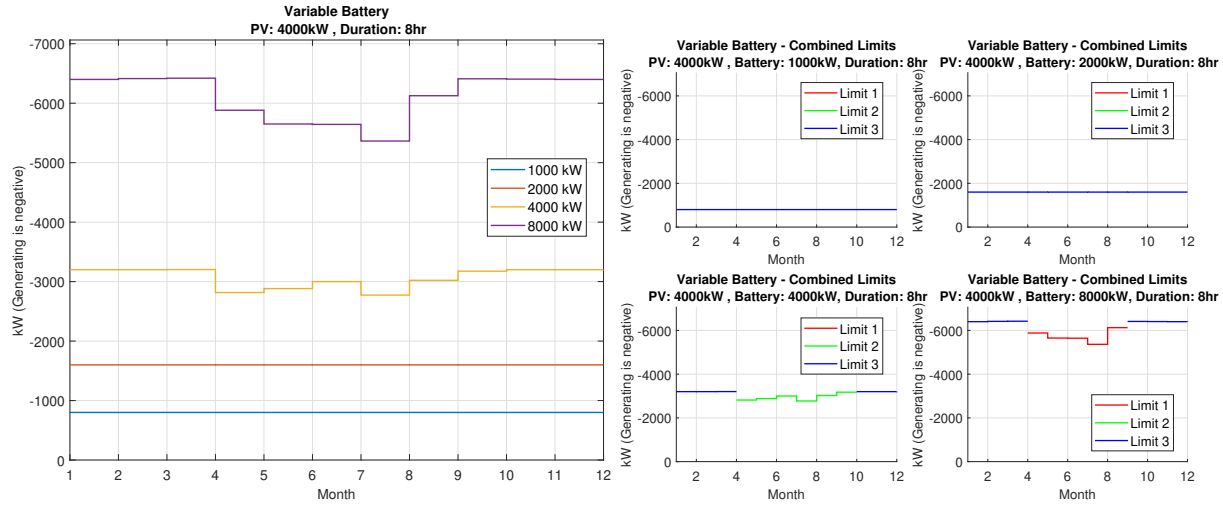

(a) (b)

Figure 3-22: (a) 4MW PV, 8hr duration, variable battery power. (b) Battery visualized by active limit.

The sizing of the PV again lines up with what has been seen previously in relation to over-sizing based on the site's grid connection. Figure 3-23 shows that when PV is over-sized relative to the grid connection, limit 3 becomes active, and dispatchable capacity is reduced with increasing PV and battery power.

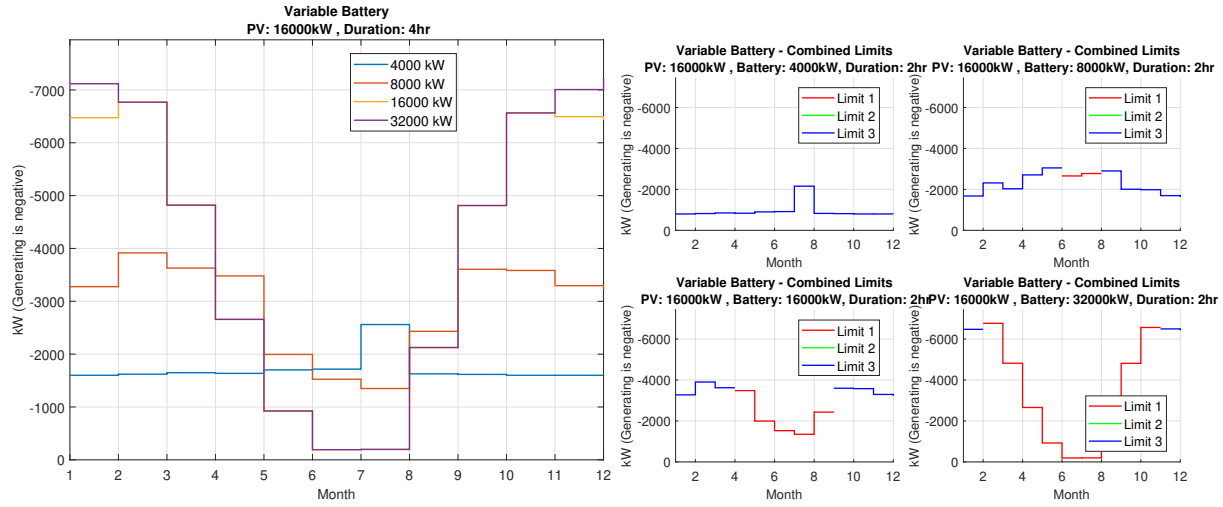

(a) (b)

Figure 3-23: (a) 16MW PV, 2hr duration, variable battery power. (b) Battery visualized by active limit.

While each of the considerations of the facility sizing can give insight into efficiencies and potential for dispatchable capacity, another element can be added to tune the facility configuration with an optimal operation—control law.

3.3.5 Comparing Control Laws and Facility Sizing

The control parameter considered in the next set of studies is reserve state of charge (SoC). For the question of dispatchable capacity, maintaining a minimum charge in the battery is a primary focus for being able to fulfill a capacity contract. The inherent trade-off of minimum reserve SoC is that it restricts the facility from providing power into the grid as wholesale energy sales during the dispatch duration, thus potentially generating less revenue from energy sales. In this comparison, a total of 510 simulations are run with parameters given in Table 6:

Table 6: Control law facility configurations.

PV Sizing (MW)	**Battery Duration (hr)**	**Battery Power 4MW PV (MW)**	**Battery Power 16MW PV (MW)**	**Reserve SoC (%)**
4	4	1.00	4	10
16		1.50	6	15
		2.00	8	20
		2.50	10	25
		3.00	12	30
		3.50	14	35
		4.00	16	40
		4.50	18	45
		5.00	20	50
		5.50	22	55
		6.00	24	60
		6.50	26	65
		7.00	28	70
		7.50	30	75
		8.00	32	80
				85
				90

For the cases chosen to analyze through simulation, a PV power sizing of 4MW and 16MW is chosen. All 510 simulation runs are considered only for site 1, given in table 5. This is the same site as previously described. This gives a PV sizing that is $\frac{1}{2}$ and 2x the maximum grid connection limit. Recalling the discussion of limit 1 in Section 3.3.1 and subsequent plots comparing active limits, the balance between

PV and battery power affects the grid's ability to accept the power generated (or not generated) by the facility. In these cases, rather than looking at each month, several facility parameters and levels of reserve SoC are considered with the months averaged. Limits are calculated as the worst of each day taken for the month, then all the months are averaged. This gives a better resolution for considering economic impact, as the contract could be negotiated for each month; so while some months maybe lower or higher, the yearly revenue is accurately reflected by the averaged months.

4MW PV

A simulation case would be a set value of PV and battery duration with variable battery power sizing and reserve SoC. These results are then plotted as a mesh plot to visualize how the combination of battery power sizing and reserve SoC affect the dispatchable capacity. The hypothesis in this plotting is that there must be some point at which there are diminishing returns for the reserve SoC in the battery versus the resultant dispatchable capacity. This is the strength of the analysis tool built as a wrap-around to the PSCG simulation. Within the simulation, a myriad of controller parameters can be adjusted, and the analysis tool can easily visualize the results to see exactly what is the outcome of the controller parameters used.

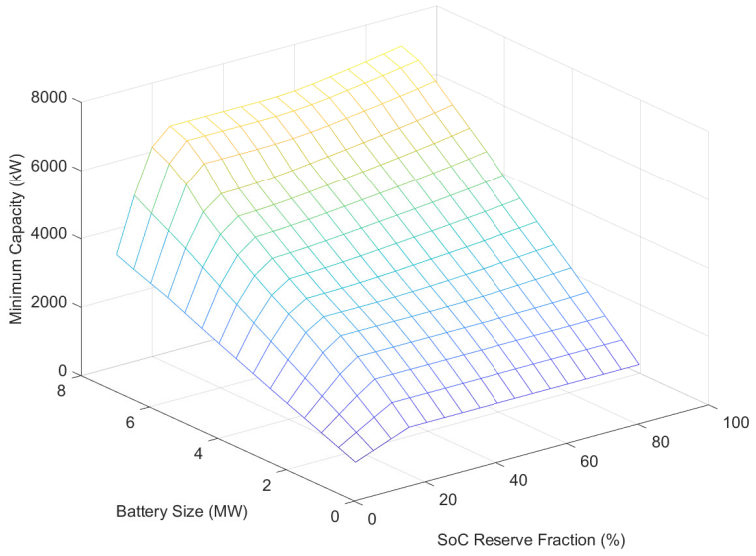

(a)

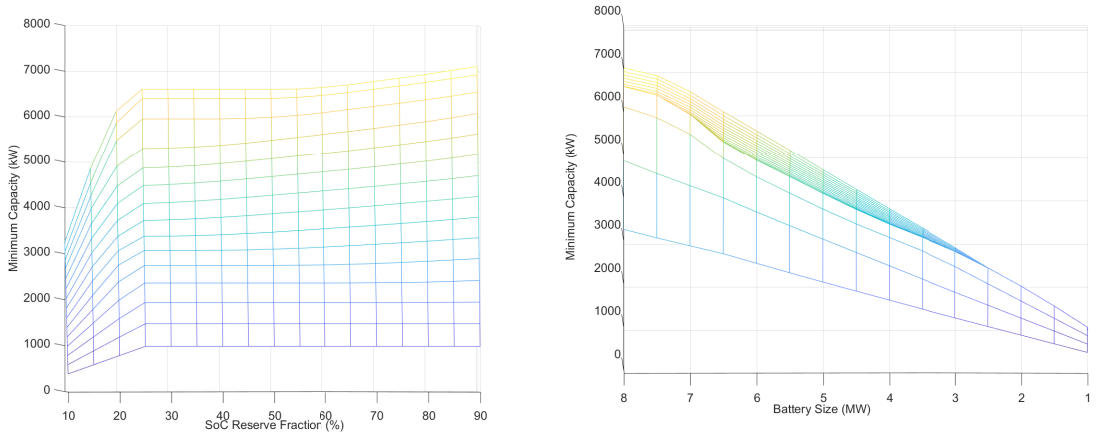

(b) (c)

Figure 3-24: (a) 4MW PV, 4hr duration, dispatchable capacity vs reserve SoC. (b) Dispatchable capacity vs reserve SoC rotated view. (c) Dispatchable capacity vs battery rotated view.

Figure 3-24 shows a 4MW PV with a sweep of battery power from 1MW to 8MW in 0.5MW increments and with a duration of 4 hours. This is then compared against a reserve SoC of 10-90% in 5% increments. The mesh plot confirms that there is in fact an optimal reserve SoC for the batteries at approximately 25%, shown in Figure 3-24b. Past this point, there is minimal increase in dispatchable capacity and, presumably, a decrease in wholesale energy sold due to reserve SoC requirements. Figure 3-24c shows the increase in the rate at which the increased reserve SoC reaches its max. This also more clearly shows the diminishing return of increased reserve SoC as any value above 25% is more compacted, plateauing in the previous view. Overall, the increase in the dispatchable capacity is only approximately 0.5MW between 25% and 90% charge reserve. The benefit of knowing where the knee of the curve is, the point at which the reserve SoC is most optimal, leads to higher revenue from a facility set up to both sell energy and provide ancillary services. In this case, the lower reserve SoC defined by the control law would lead to a higher revenue from energy sales since there would be more energy available to sell to the grid.

A deeper look into the facility's performance at each parameter gives an indication as to what is determining the limit of the dispatchable capacity. Figure 3-25 shows the most active limit for each of the simulated runs where limit 1 is purple, limit 2 is cyan, and limit 3 is yellow. At a low reserve SoC and any battery power size, limit 3, the energy in the battery, is the active limit. This is expected for the site sizing. As the reserve SoC increases, the limit becomes limit 2, the battery power electronics. Once the largest battery power size for this case is considered, the limit in effect is limit 1, the grid connection. This again points to the knee of the previous curve as a 25% reserve SoC with an 8MW battery, giving the only limit in effect as the grid connection while maximizing the dispatchable capacity.

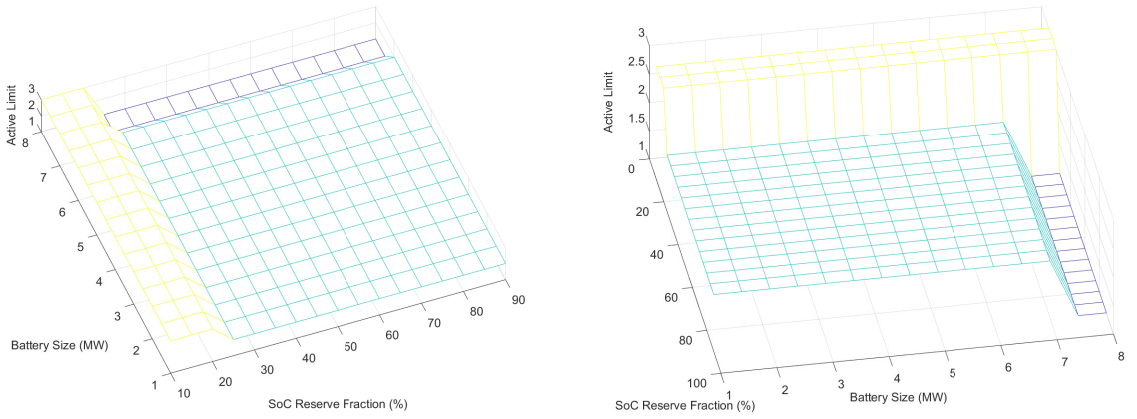

(a) (b)

Figure 3-25: (a) 4MW PV, 4hr duration, dispatchable capacity vs reserve SoC, active limit. (b) Active limit, rotated view.

It should be noted in the case of 4MW PV there is no curtailment during the simulation, which also supports the usage of a smaller PV relative to the grid connection limit, as there is less energy wasted during the year due to a saturated grid connection or full battery.

16MW PV

Comparing results for the 16MW PV sizing, the over-sizing of the PV leads to the facility doing a considerable amount of curtailment due to saturating the grid connection. Figure 3-26 shows the minimum dispatchable capacity for battery power of 4MW, 6MW, and 8-32MW. Large battery with low reserve SoC ends up discharging most of the energy into the grid, again saturating the grid connection until the reserve SoC becomes high enough to keep the excess energy from the PV in the battery. Even in this case, the dispatchable capacity is significantly lower than using a 4MW PV for cases of small battery power with a reserve SoC higher than 80%.

Figure 3-27b and 3-27c show what is expected of the large PV with large battery, in that the limit in effect is the grid connection (limit 1) for nearly every case except small battery and high reserve SoC. In these cases it is the battery power that is constraining the dispatchable capacity, the exception being the small portion that is shown for 10MW-20MW battery with little reserve SoC.

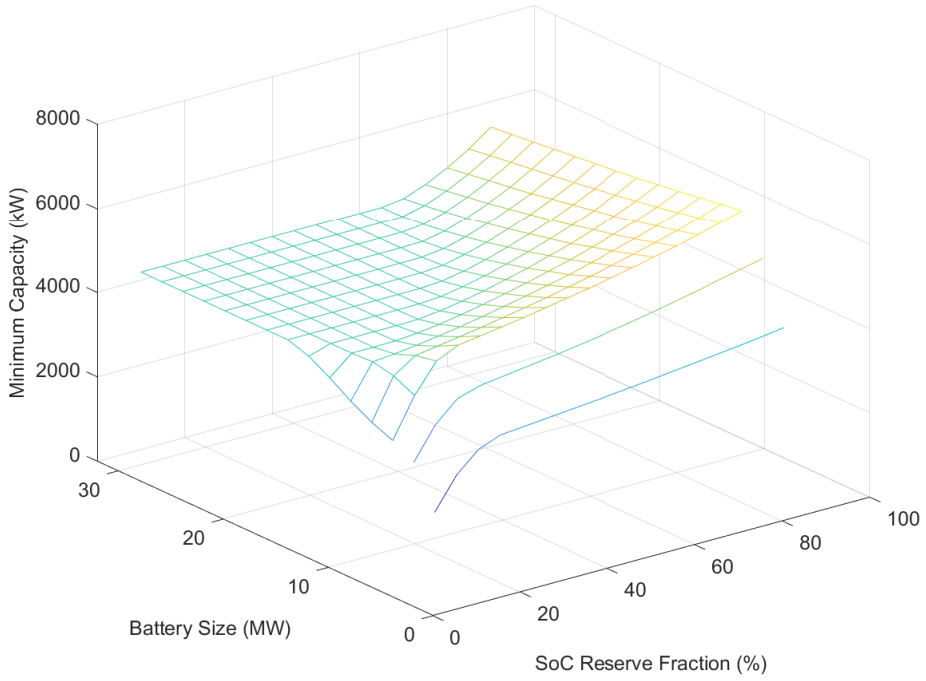

Figure 3-26: 16MW PV, 4hr Duration, large battery power vs reserve SoC.

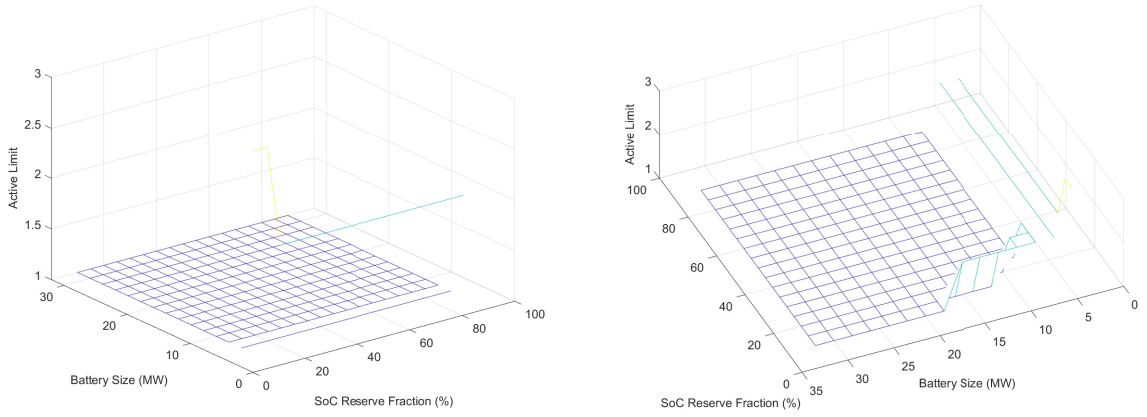

(a) (b)

Figure 3-27: (a) 16MW PV, 4hr duration, dispatchable capacity vs reserve SoC, active limit. (b) Active limit, rotated view.

Based on the findings of the larger battery with 16MW PV, another simulation is run with smaller battery power sizes paired with the 16MW PV, this time with battery power ranging from 0.25MW to 8MW to show the steps between the battery power sizing, shown in Figure 3-28. Compared to Figure 3-26, this

would be the back half of mesh plot, forming a hill with the peak at 8MW battery with 90% reserve SoC. This result is considerably different from the lower 4MW PV case where the peak of the mesh was at 8MW and 25% reserve SoC. In this case, however, the larger PV would give way to higher revenue from selling power during off-contract times.

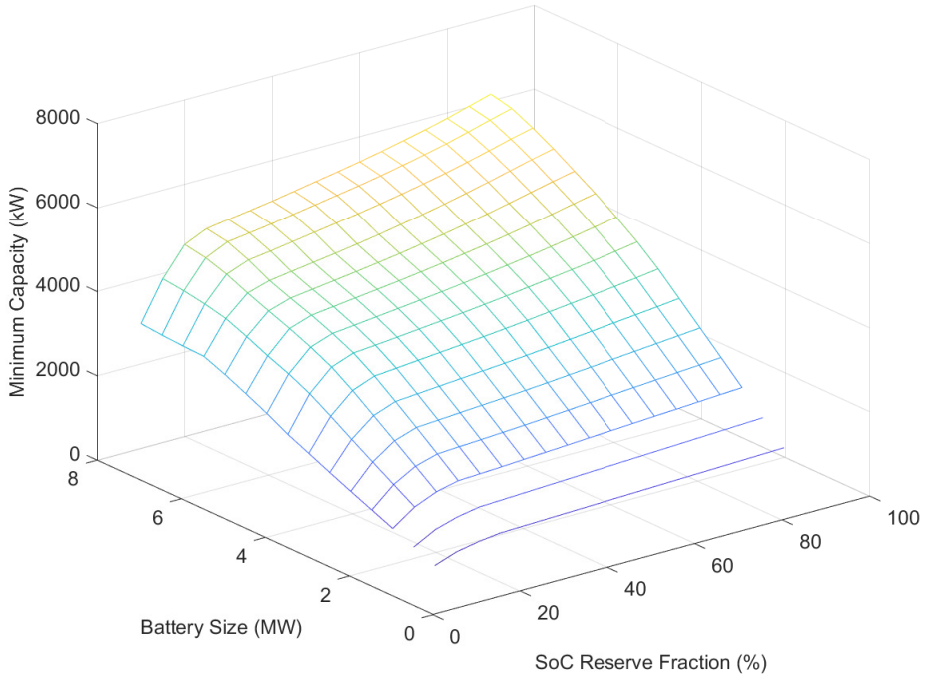

Figure 3-28: 16MW PV, 4hr duration, small battery power vs reserve SoC.

Figure 3-29 also helps make sense of the mesh peak for the smaller battery cases. With little battery power and low reserve SoC, it makes sense the limit would be the stored battery energy, while the battery power electronics become the dominant limit as battery power increases and reserve SoC is increased. Finally, limit 1, the grid connection, becomes the constraining factor to dispatchable capacity at 16MW PV for nearly all of the 8MW battery's reserve SoC cases.

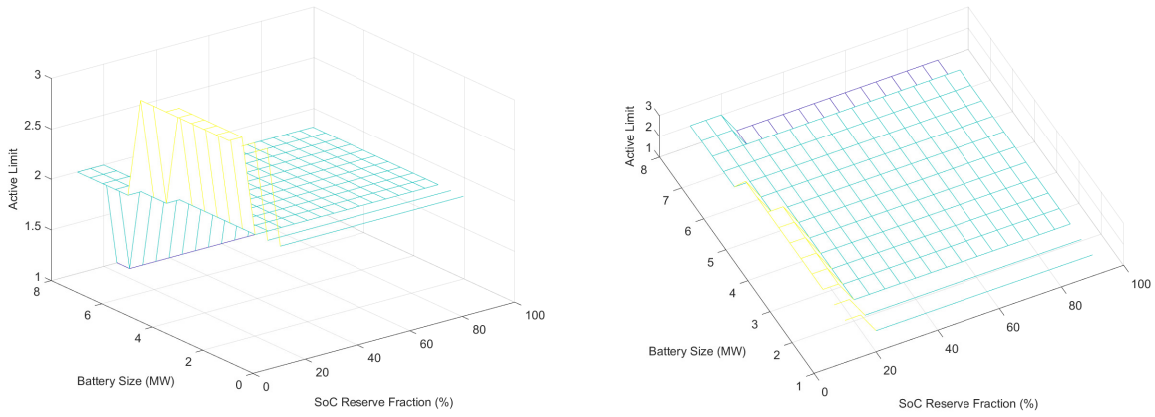

(a) (b)

Figure 3-29: (a) 16MW PV, 4hr duration, dispatchable capacity vs reserve SoC, active limit (b) Active limit, rotated view.

3.3.6 Weibull Distribution for Confidence

Previous limit calculations used a method of taking the worst day of each month, and the average of all 12 months. A more robust and statistical method should be utilized to more accurately predict the facility's response. For this, a Weibull distribution is used to calculate confidence of minimum dispatchable capacity. The Weibull fit is given by [33]

$$\begin{aligned} F(x) &= 1 - e^{-(\frac{x}{\alpha})^{\beta}} \\ 1 - F(x) &= e^{-(\frac{x}{\alpha})^{\beta}} \end{aligned} \tag{14}$$

where $e^{-(\frac{x}{\alpha})^{\beta}}$ is the reliability function and $F(x)$ is the cumulative distribution function with α and β being the shape and scale of the Weibull fit. Once the fit is made, a Weibull inverse is made using two confidence levels, 99.9% and 99.9999%, P_1 and P_2.

$$x = F^{-1}(P|_{\alpha,\beta}) = -\alpha[ln(1-P)]^{\frac{1}{\beta}} \tag{15}$$

The values of dispatchable capacity for each yearly run are grouped by the 6-hour contract interval within each month and arranged in descending power. The Weibull distribution is fit to the data, and the inverse is run at each confidence level. There are two main issues with fitting the Weibull distribution. The first is when there are multiple peaks towards the low end of the power range. For this, the peak of the distribution is shifted to the next peak in the distribution and the process reiterated.

An example is shown in Figure 3-30. The cyan cross shows the 99.9% power level and the red cross shows the 99.9999% level. Since there are only approximately 11,000 points to the sample data, there should rarely be any values after the 99.9999% confidence point. Zooming in on the data in Figure 3-30b shows that there are 3 points past the 1:1,000,000 confidence level. One observation is that there are multiple processes present, giving multiple peaks. These may correspond to various operating conditions, sunny or cloudy days (impacting feeder loads as well as PV generation, with feeder load substantially impacting limit 1), or may correspond to different states of the load tap changer. Of interest is the process giving the distribution at the right-hand edge. An effort is made to fit the right-most process by selecting a subset of the right most points, shown in Figure 3-31.

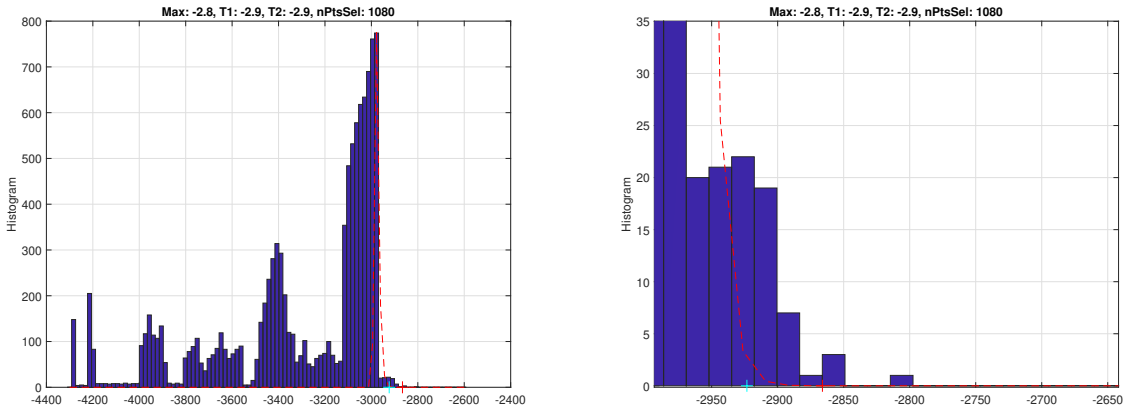

(a) (b)

Figure 3-30: (a) Weibull distribution fit with tail presence. (b) Zoomed to show tail.

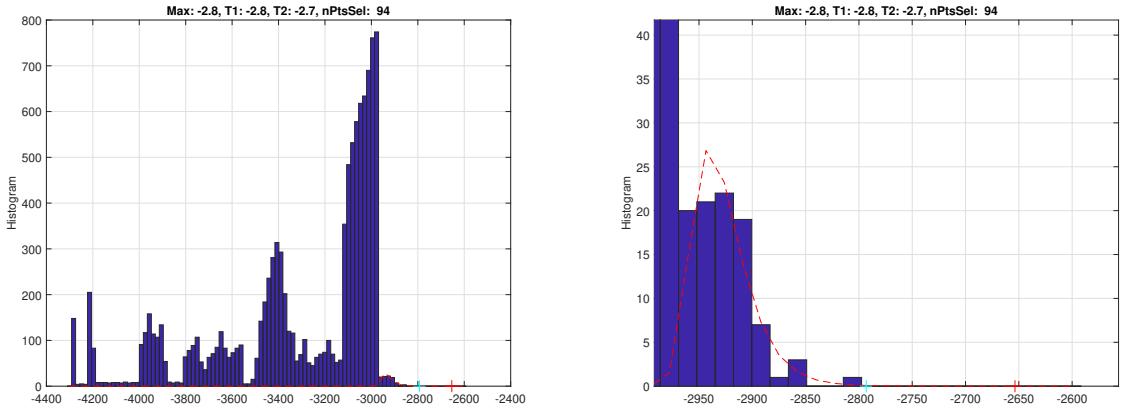

(a) (b)

Figure 3-31: (a) Weibull distribution fit with tail presence - shifted. (b) Zoomed to show tail.

The other issue encountered is an edge case where the tail is exceedingly long and the Weibull distribution is a poor choice for fitting the data, such as in Figure 3-32. In this case, there is no suitable peak further towards the low end of the power and, as seen in Figure 3-32b, the 99.9999% point has several points to the right. A simplified solution, shown in Figure 3-32c, chooses the furthest point as the 99.9999% point. This is more conservative than required, but in total, this edge case happens 54 times among the 510 cases, giving 54 points out of 5,691,600 points (510 x 11,160). Considering the edge cases for the tails versus the total amount of points, approximately 99.9999% of the points are above the minimum expected.

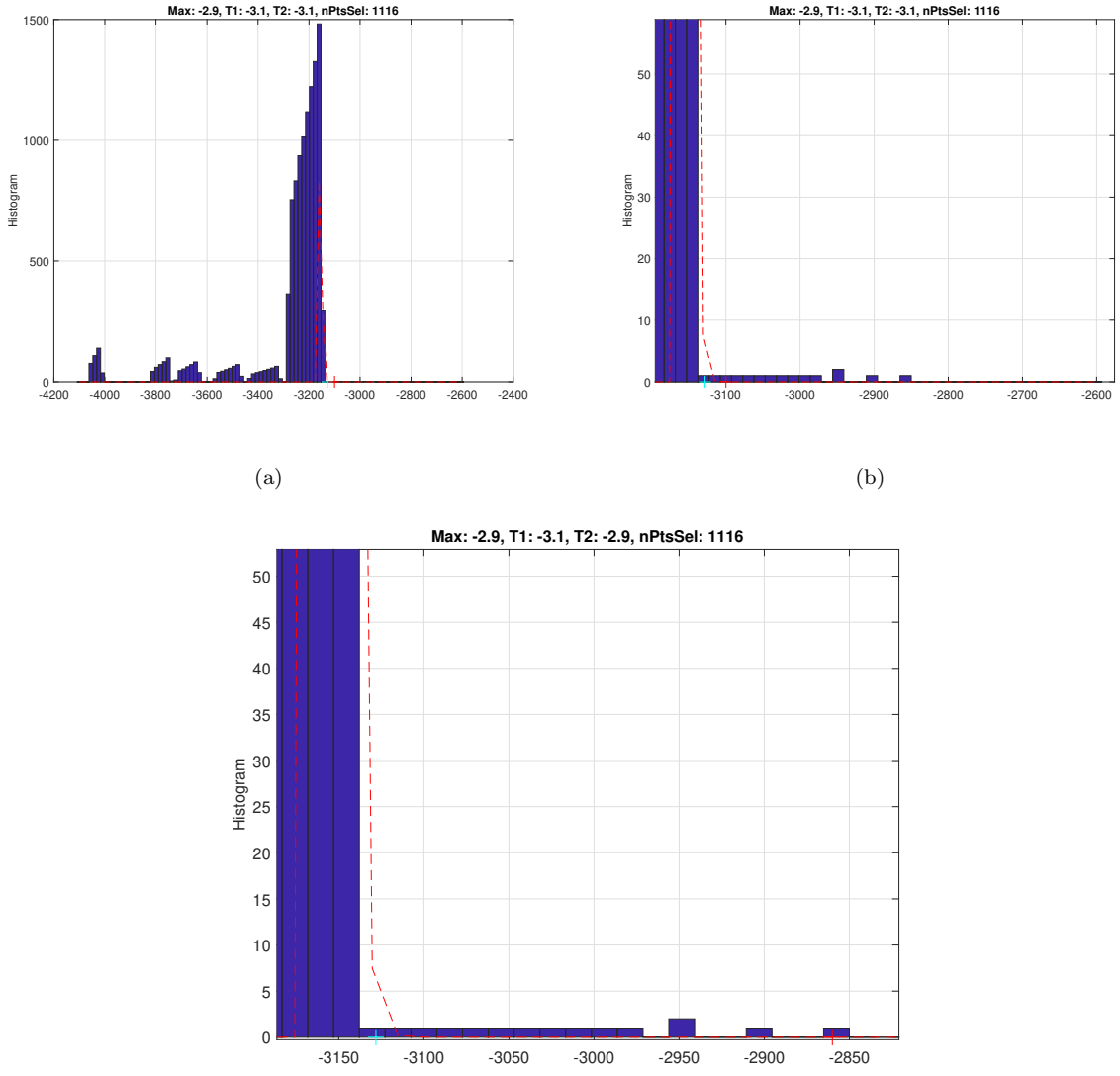

(a)

(b)

(c)

Figure 3-32: (a) Weibull distribution fit with tail presence - shifted. (b) Zoomed to show tail. (c) Shifted 99.9999% confidence point.

Results of the Weibull distribution are shown in Figures 3-33, 3-34, and 3-35. These are the comparisons to Figures 3-24, 3-26, and 3-28, respectively. As to be expected, each Weibull plot approximately matches the shape of the comparison plot. For the 4MW PV case, the 99.9% confidence plot is at approximately the same level of the averaged dispatchable capacity while the 99.9999% is slightly lower, as to be expected. The 16MW PV case, however, shows both confidence levels lower than the average which can points to a result of averaging large differences of dispatchable capacity in summer months compared to the rest of the year.

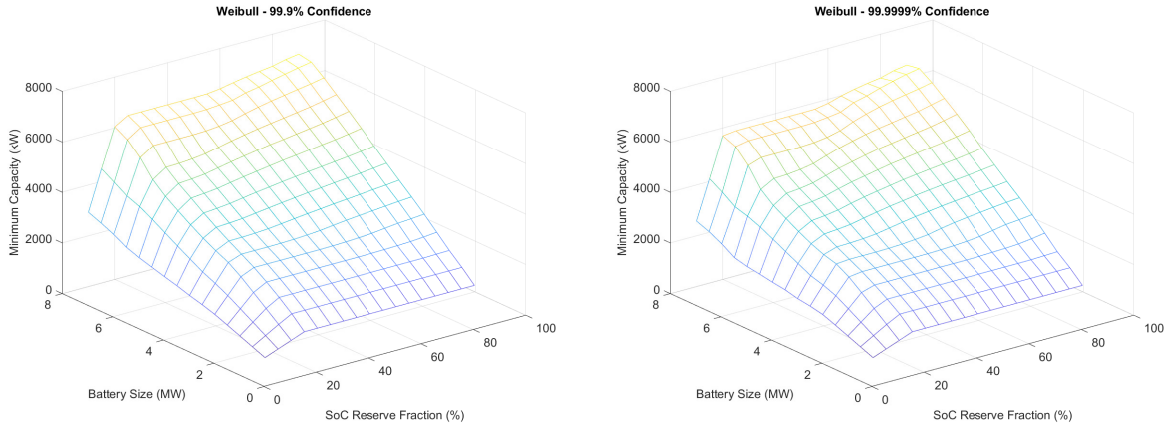

(a) (b)

Figure 3-33: (a) Weibull confidence, 99.9% - 4MW PV, battery power vs reserve SoC. (b) Weibull confidence, 99.9999%.

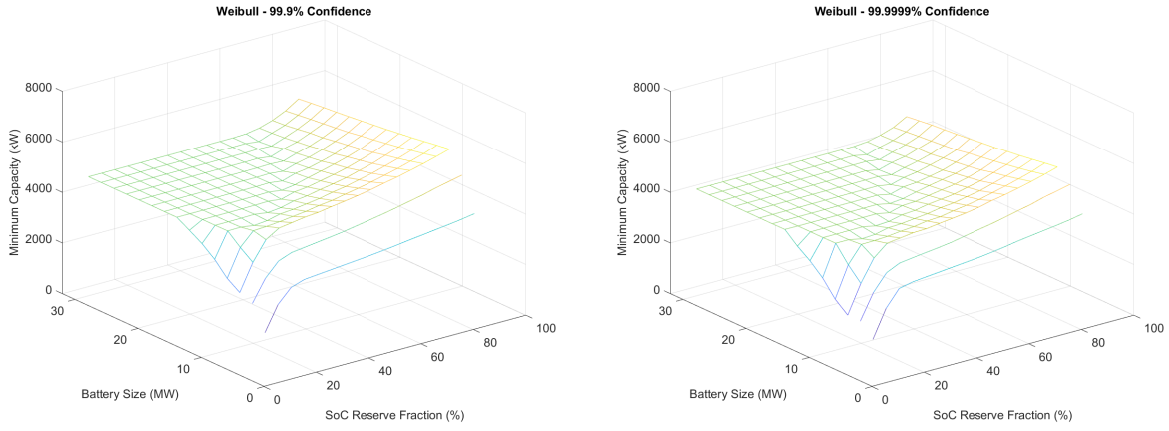

(a) (b)

Figure 3-34: (a) Weibull confidence, 99.9% - 16MW PV, large battery power vs reserve SoC. (b) Weibull Confidence, 99.9999%.

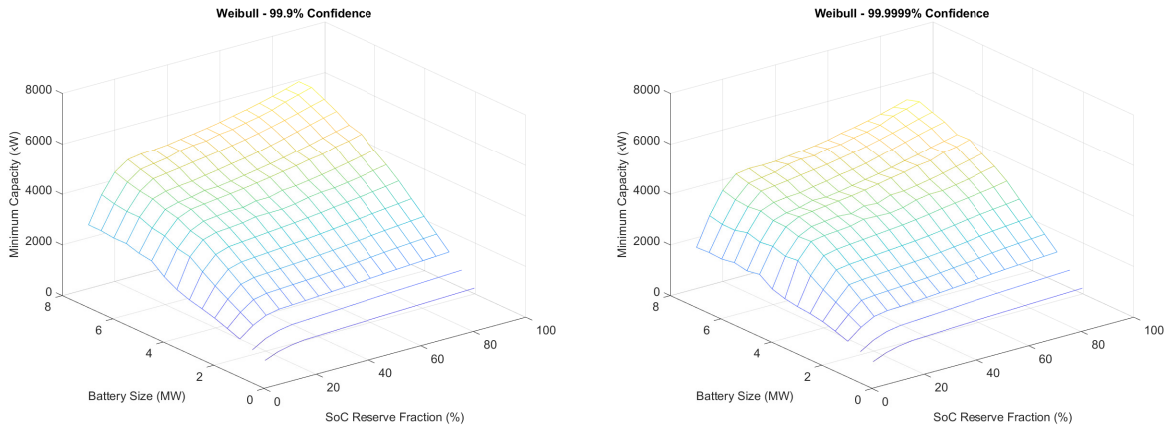

(a) (b)

Figure 3-35: (a) Weibull confidence, 99.9% - 16MW PV, small battery power vs reserve SoC. (b) Weibull confidence, 99.9999%.

The important factor of the Weibull distribution, as stated earlier, is that it provides a robust statistical method for determining the dispatchable capacity of each case. It is also important to note that the confidence level, like most of the simulation and analysis tool, is adjustable. Contract penalties are outside the scope of this work, but there can be a balance between the confidence level and the revenue generated by pushing the confidence lower, thus increasing the projected dispatchable capacity and revenue.

3.3.7 Economic Impact of Facility Sizing

The last portion of the work is an examination of the economic impact of each facility size. Pricing is pulled for the cost of solar per kW, battery power electronics per kW, and battery duration sizing per kWh, shown in Table 7. Yields are based on figures from Nelson *et al.* [22] and PV cost from Jaganmohan [34].

Table 7: Cost and yield pricing for PV and battery facility.

Cost			**Yield**	
PV ($/kW)	$883		Direct Yield ($/MWh)	$30
Battery ($/kW)	$50		Indirect Yield ($/MWh)	$50
Battery Duration($/kWh)	$130		Dispatchable Capacity ($/MW-day)	$313

The goal is to examine where the optimal point is for battery power and control law parameters across the

runs. The plots are separated into several key performance metrics for each facility size with an included contour plot of the % Yield as ROI. There are three yields considered. First, direct yield is energy delivered into the grid directly from the PV, sold at the lowest rate. Second, an indirect battery discharging yield is sold at a higher rate as it can be selectively discharged into the grid during peak times. Lastly, dispatchable capacity yield is revenue generated via capacity contract. The assumption is that at some point the contour will close, giving an ideal sizing of PV, battery power, battery duration, and reserve SoC.

Figure 3-36 shows % yield of the 4MW facility with battery power ranging from 0.25MW to 8MW. In this case, the facility actually generates the most income from a higher reserve SoC, but only marginally, with most benefit achieved by at least 30% reserve SoC. If viewed as a mesh plot, the left side of the contour would be a cliff with the right side being a plateau. Both aspects of the contour plot line up with the dispatchable capacity mesh from Figure 3-24, where the knee of the curve is at 25% reserve SoC with a marginal increase past 25%. This also points to the fact that a good portion of the total yield is coming from the dispatchable capacity yield. With only a marginal increase in the % yield from increased reserve state of charge, it is feasible for the facility to operate in a wide range of reserve SoC with battery power between 4MW and 8MW.

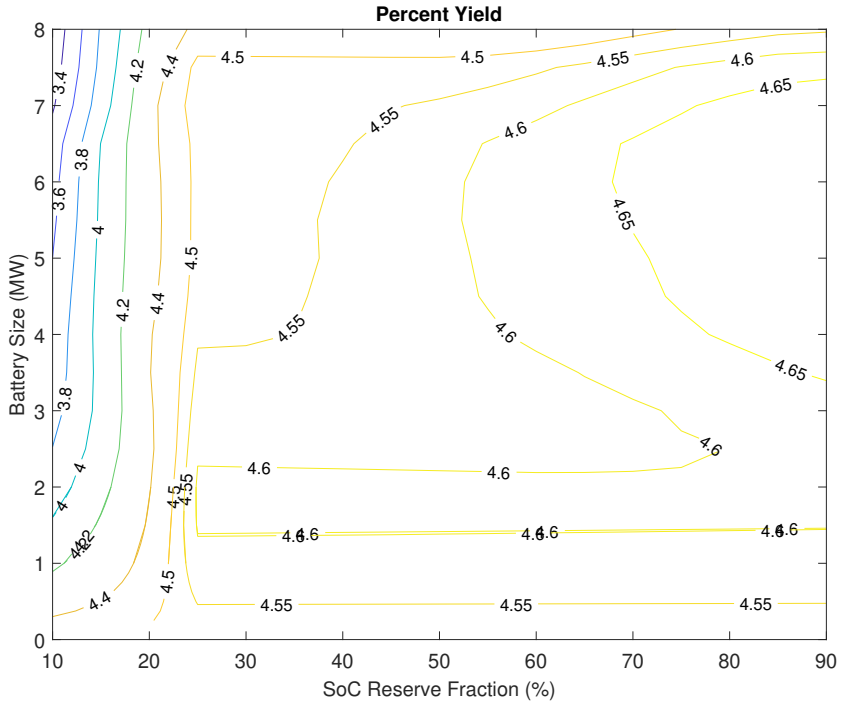

Figure 3-36: % Yield of 4MW PV facility as contour (artifact at 4.6%).

Examining the split of yields in Figure 3-37, dispatchable capacity dominates the yield of the 4MW PV

facility by nearly the direct and indirect yield combined. The yield rates can of course be modified to adjust for decreases in PV and battery costs as previously discussed, or a worst-case scenario to further identify the most optimal facility size and reserve SoC control law.

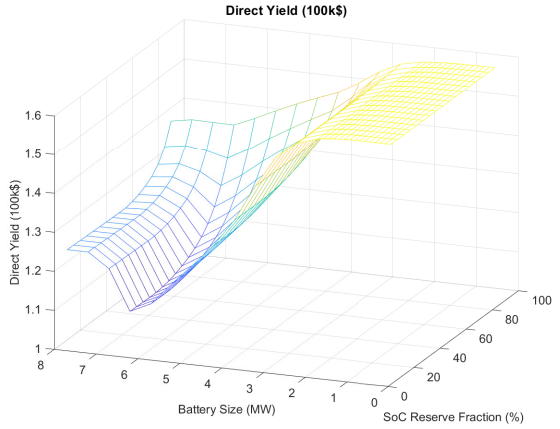

(a)

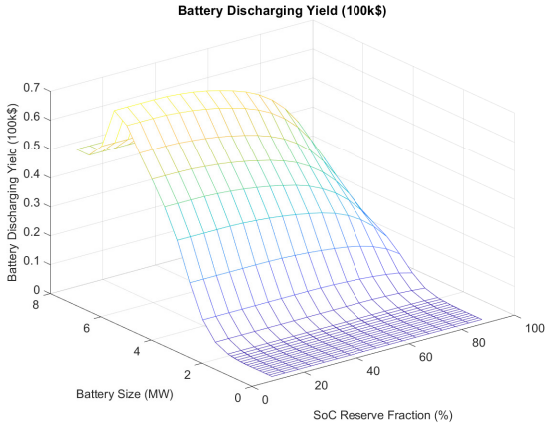

(b)

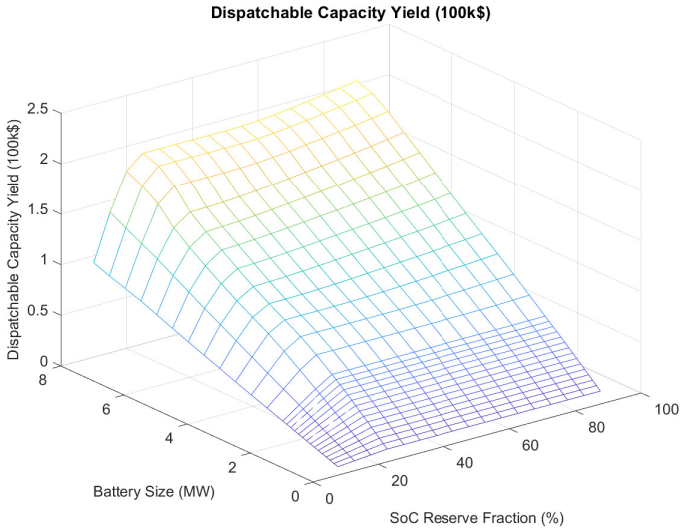

(c)

Figure 3-37: (a) 4MW facility direct yield. (b) 4MW battery discharging yield. (c) 4MW dispatchable capacity yield.

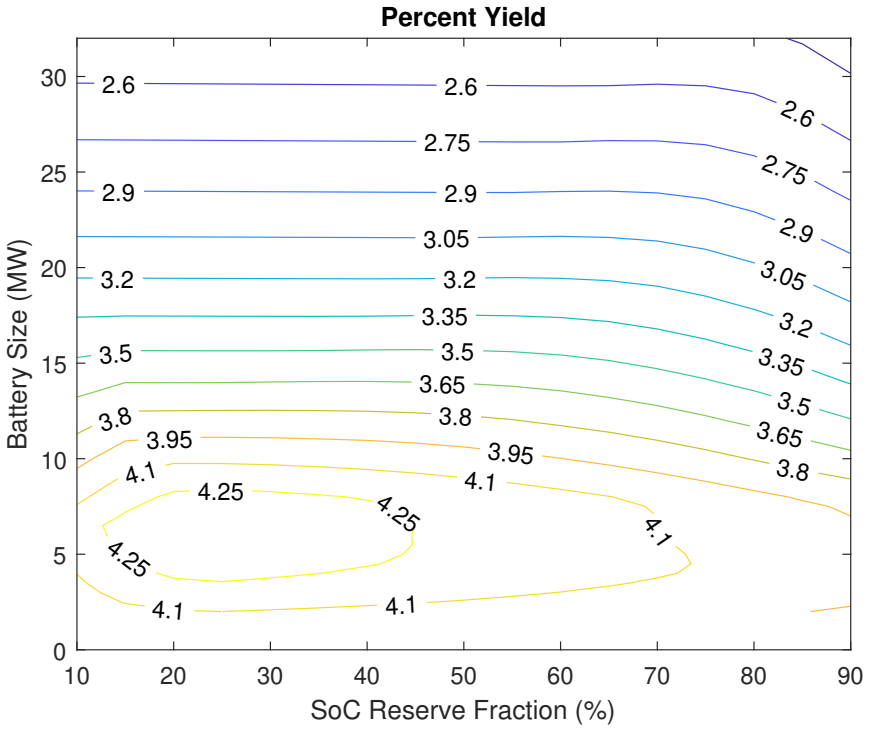

Figure 3-38: % Yield of 16MW PV facility.

The yield plot for the 16MW PV facility is quite different from that of the 4MW facility. In this case, a smaller battery of approximately 6-8MW with a 25% reserve gives the best % yield, shown in Figure 3-38. While the % yield is not as high as the 4MW facility, the total yearly yield in US dollars ($) is over double that of the 4MW facility, with the 16MW PV facility at an approximately $800k per year yield compared to the 4MW facility's $375k. Noting previously from Figure 3-26 and 3-28, the knee of the dispatchable capacity was 25% reserve SoC and in the range of 8MW battery power.

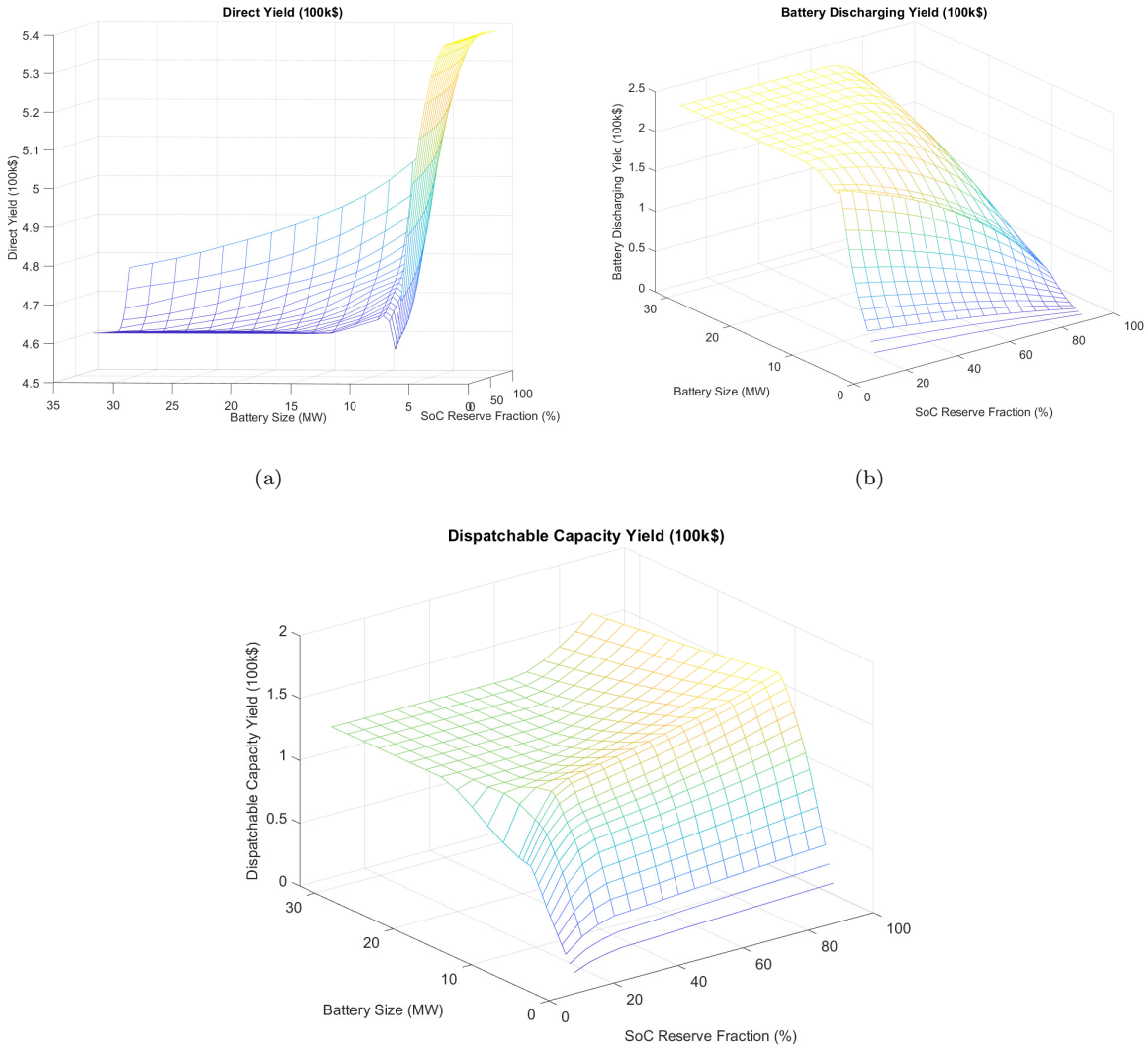

(a) (b)

(c)

Figure 3-39: (a) 16MW facility direct yield. (b) 16MW battery discharging yield. (c) 16MW dispatchable capacity yield.

In this case, however, the direct yield has a steep decline of about 10% as the battery power increases, giving lower direct yield while the battery discharging yield rises and dispatchable capacity plateaus. Due to the over-sizing of the PV, the 16MW facility can curtail, with the majority of the curtailing happening with battery power less than 8MW or greater than 30% reserve SoC. Battery power larger than 8MW offsets the gain from the dispatchable capacity due to cost of the battery duration. Likewise, the grid connection limits the dispatchable capacity maximum to just below the grid connection limit, approximately 7MW. This makes the larger batteries a detriment to the system because of their cost and, for the same reason, makes the direct yield the dominating portion of the total yield.

The following figures show a benefit of the simulation and analysis tool. Costs and yields can be adjusted to see the outcome of % total yield and to see the most efficient build of a future facility based on trends of PV and battery costs. It is understandable that if PV and battery decrease linearly together, the % yield will increase but the focus of the contour will remain unchanged. If one changes without the other, such as in Figure 3-40 showing a halved cost of PV at $443 per kW for a 16MW facility, the focus of the contour shifts downward, making battery storage unnecessary in relation to % yield. In other words, the facility functions more profitably with no battery at all. This is due to the direct yield being the dominating yield for the facility and the dispatchable capacity yield unable to compensate battery duration cost compared to the decreased cost of PV. The dispatchable capacity and battery discharge yields contribute a small enough portion to the total yield that the battery is not worth the investment.

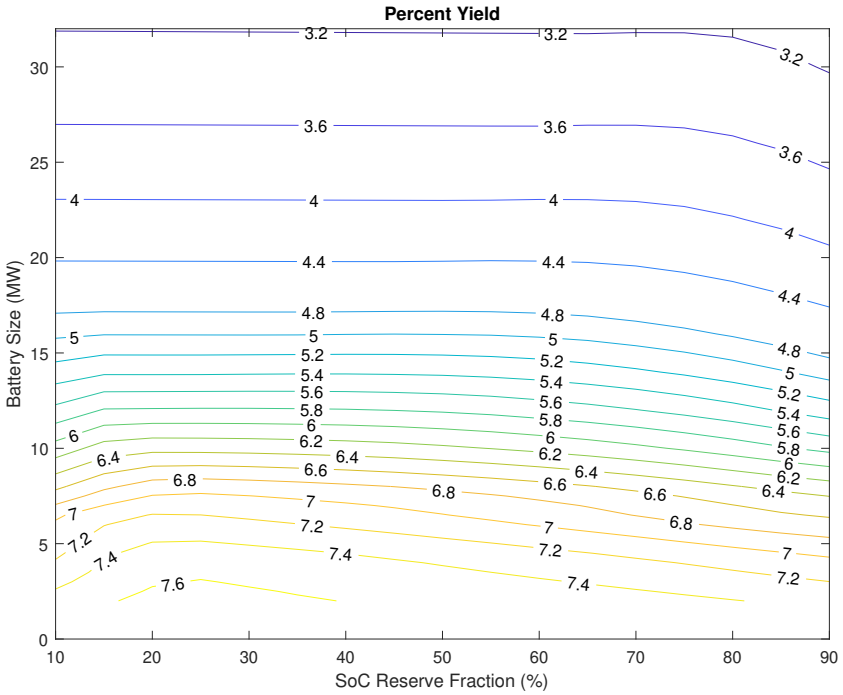

Figure 3-40: % yield of 16MW PV facility, halved cost of PV.

Comparing a similar case in the 4MW facility where the battery duration price is halved, giving a lower cost to yield ratio since dispatchable capacity yield is dominant, the contour shifts little from the original battery cost case. In Figure 3-41, the contours show less of a plateau than in Figure 3-36, giving a more focused contour center, showing that the yield of the dispatchable battery and battery discharging justify a larger battery with just as high a reserve state of charge.

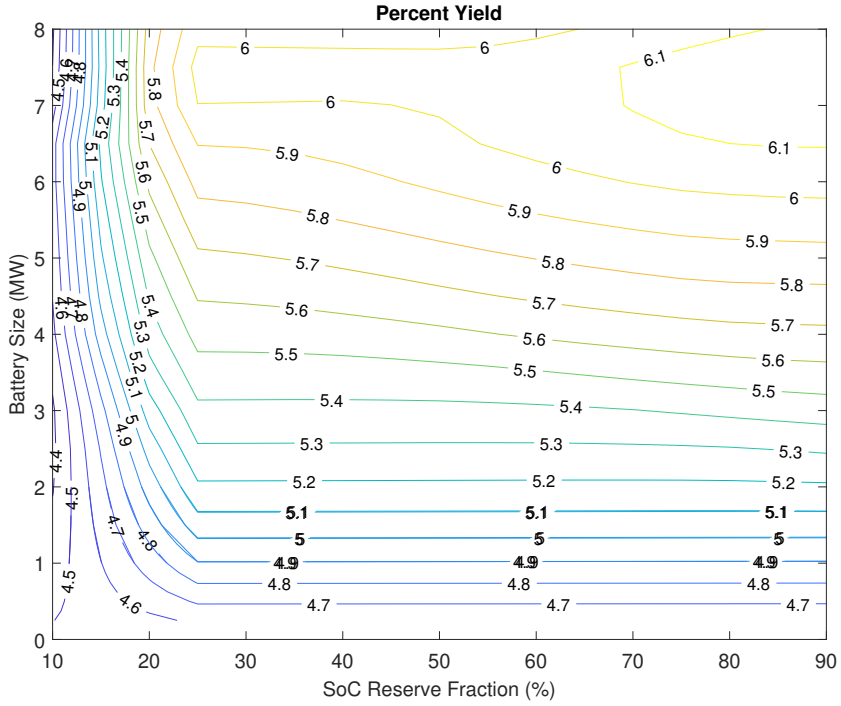

Figure 3-41: % yield of 4MW PV facility, halved cost of battery duration.

This analysis can be continued for varying cases of cost and yield, giving an accurate representation of the facility's cost to revenue in the event of changing costs and yields for future facilities.

4 Conclusion

Through various developmental stages, an analysis tool has been built to accurately predict the response of a grid with a PV and battery storage facility at a specific site with a known grid connection MVA limit. Since PV and battery facilities are generally located in remote areas, it is important to consider the effect of weak feeders within the grid where the facility is connected. Using real solar data, real load data, an accurately modeled load tap changer, variable facility parameters, and variable control laws, effectiveness of the facility can be accurately modeled within a selected confidence taking into consideration the site connection and grid response. Focusing on a 4MW and 16MW PV facility at a site with an 8MVA connection limit, it can be shown that there is, in fact, an optimal facility sizing with tuned control laws. In this case, the sizing of the PV has a widely varying affect on the % yield from the facility. In the end, appropriately sized PV with a battery gives the highest yield, though the control laws would need to be adjusted for each of the PV sizes.

The end goal of this analysis tool is to show, not just the effect of the parameters tested within this thesis, but that virtually any parameter can be tweaked and an accurate representation of the site and grid's response can be modeled. A constraint enforcing controller such as the one used in this simulation compared to a model predictive controller is a question that can feasibly be answered, including the effect of different weights and costs within each controller. The level of detail of the simulation that the analysis tool can visualize and the accuracy and confidence at which it produces results provides a strong case for the viability of dispatchable capacity as a source of revenue for PV and battery facilities.

5 Future Work

The modular build of the PSCG simulation and the accompanying analysis tool developed in this thesis provides a great deal of flexibility for future work. Prior simulations that were not the focus of this thesis included two other sites; particularly of interest is a 20MVA grid connection site. Since most of the dispatchable capacity limits came down to grid connection, it would be beneficial to see how the 20MVA site would respond to limits of similar systems. The split of PV sizing versus battery power (0.5, 1x, 2x, etc.) was intentional as a way to look at other sites as well. It is likely that sites that have similar feeder line impedance would behave similarly, showing a trend in optimal PV and battery energy based on grid connection.

The analysis tool would need to be adapted for each variable parameter added to the PSCG simulation. There are dauntingly numerous combinations of controllers and controller parameters that would significantly change the outcome of each simulation run. This tool would also provide a way to accurately predict and therefore justify the use of novel controllers in new or retrofitted PV and battery facilities such as the controller presented by Nelson *et al.* [22]. Therefore, making the adaptation dynamic would provide more flexibility for visualizing changes to the simulation.

Lastly, adding in systematic predictions of PV and battery pricing such as work done by Ziegler and Trancik[31], Frazier *et al.* [26], and Curry [4] that can be integrated into the economic output would help to further explore the economics of capacity contracts. Likewise, capacity contract pricing was difficult to find and settled for sourcing from other papers rather than specifically from MISO. Coupling the future demand for ancillary services with real contract prices would also make for a strong case of the analysis tool to accurately predict viability as a function of capacity contract pricing changes.

REFERENCES

[1] DNV GL Digital Solutions, *"User Guide Synergi Electric 6.5.0,"* DNV GL AS., March, 2020.

[2] S. Chatradi, N. Giovannetti, A. Nasiri, B. Armstrong *"PSCG: Synergy Electric based PV + Storage + Control + Grid Modeling,"* DNV 2021 Electric Grid User Seminar, DNV, Virtual, 10:30-11:00AM CST, September 29, 2021.

[3] M. Bollen and F. Hassan, *"Integration of distributed generation in the power system,"* Hoboken: IEEE Press, 2011.

[4] C. Curry, *"Lithium-ion Battery Costs and Market,"* Bloomberg New Energy Finance, July 2021.

[5] F. O. Hocaoglu, F. Serttas, *"A novel hybrid (Mycielski-Markov) model for hourly solar radiation forecasting,"* Renewable Energy, Volume 108, 2017, Pages 635-643, ISSN 0960-1481, https://doi.org/10.1016/j.renene.2016.08.058.

[6] National Solar Radiation Database, *"What is the NSRDB?,"* NSRDB. [Online]. Available: https://nsrdb.nrel.gov/.

[7] T. Bowen, I. Chernyakhovskiy, P. Denholm, *"Grid-Scale Battery Storage FAQ - NREL,"* September, 2019.

[8] J. Polo, L.F. Zarzalejo, R. Marchante, A.A. Navarro, *"A simple approach to the synthetic generation of solar irradiance time series with high temporal resolution,"* Solar Energy, Volume 85, Issue 5, 2011, Pages 1164-1170, ISSN 0038-092X, https://doi.org/10.1016/j.solener.2011.03.011.

[9] R.J. Aguiar, M. Collares-Pereira, J.P. Conde, *"Simple procedure for generating sequences of daily radiation values using a library of Markov transition matrices,"* Solar Energy, Volume 40, Issue 3, 1988, Pages 269-279, ISSN 0038-092X, https://doi.org/10.1016/0038-092X(88)90049-7.

[10] W. Zhang, W. Kleiber, A. R. Florita, B. Hodge and B. Mather, *"Modeling and Simulation of High-Frequency Solar Irradiance,"* in IEEE Journal of Photovoltaics, vol. 9, no. 1, pp. 124-131, Jan. 2019, doi: 10.1109/JPHOTOV.2018.2879756.

[11] J. Munkhammar, J. Widén, *"A Markov-chain probability distribution mixture approach to the clear-sky index,"* Solar Energy, Volume 170, 2018, Pages 174-183, ISSN 0038-092X, https://doi.org/10.1016/j.solener.2018.05.055.

[12] J.M. Bright, C.J. Smith, P.G. Taylor, R. Crook, *"Stochastic generation of synthetic minutely irradiance time series derived from mean hourly weather observation data,"* Solar Energy, Volume 115, 2015, Pages 229-242, ISSN 0038-092X, https://doi.org/10.1016/j.solener.2015.02.032.

[13] B.O. Ngoko, H. Sugihara, T. Funaki, *"Synthetic generation of high temporal resolution solar radiation data using Markov models,"* Solar Energy, Volume 103, 2014, Pages 160-170, ISSN 0038-092X, https://doi.org/10.1016/j.solener.2014.02.026.

[14] M. Reno, C. Hansen, *"Identification of Periods of Clear Sky Irradiance in Time Series of GHI Measurements,"* Renewable Energy, 2016, 90.10.1016/j.renene.2015.12.031.

[15] C.- C. Liu and K. T. Vu, *"Analysis of tap-changer dynamics and construction of voltage stability regions,"* in IEEE Transactions on Circuits and Systems, vol. 36, no. 4, pp. 575-590, April 1989, doi: 10.1109/31.92890.

[16] B. Kasztenny, E. Rosolowski, J. Izykowski, M. M. Saha and B. Hillstrom, *"Fuzzy logic controller for on-load transformer tap changer,"* in IEEE Transactions on Power Delivery, vol. 13, no. 1, pp. 164-170, Jan. 1998, doi: 10.1109/61.660874.

[17] J. Marcos, O. Storkël, L. Marroyo, M. Garcia, E. Lorenzo, *"Storage requirements for PV power ramp-rate control,"* Solar Energy,Volume 99,2014,Pages 28-35, ISSN 0038-092X, https://doi.org/10.1016/j.solener.2013.10.037

[18] United States of America Federal Energy Regulatory Commission, *"Electric Storage Participation in Markets Operated by Regional Transmission Organizations and Independent System Operators,"* 2018.

[19] P. Hoffman, D. Streit, *"United States Electricity Industry Primer,"* Off. Electr. Deliv. Energy Reliab. U.S. Dep. Energy, DOE/OE-0017, no. July; 2015. p. 1–94. doi: DOE/ OE-0017

[20] T. Bowen, I. Chernyakhovskiy, P. Denholm, *"Grid-Scale Battery Storage Frequently Asked Questions,"* National Renewable Energy Laboratory, September, 2019.

[21] Midcontinent Independent System Operator, *"2020/2021 Planning Resource Auction (PRA) Results,"* 2020.

[22] J. R. Nelson, N. G. Johnson, *"Model predictive control of microgrids for real-time ancillary service market participation,"* Applied Energy, Volume 269, 2020.

[23] R. Sioshansi, S. H. Madaeni, P. Denholm, *"A Dynamic Programming Approach to Estimate the Capacity Value of Energy Storage,"* in IEEE Transactions on Power Systems, vol. 29, no. 1, pp. 395-403, Jan. 2014, doi: 10.1109/TPWRS.2013.2279839.

[24] R. Sioshansi, P. Denholm, T. Jenkin, J. Weiss, *"Estimating the value of electricity storage in PJM: Arbitrage and some welfare effects,"* Energy Economics, Volume 31, Issue 2, 2009, Pages 269-277, ISSN 0140-9883, https://doi.org/10.1016/j.eneco.2008.10.005.

[25] S. H. Madaeni, R. Sioshansi and P. Denholm, "Comparing Capacity Value Estimation Techniques for Photovoltaic Solar Power," in IEEE Journal of Photovoltaics, vol. 3, no. 1, pp. 407-415, Jan. 2013, doi: 10.1109/JPHOTOV.2012.2217114.

[26] A. W. Frazier, W. Cole, P. Denholm, D. Greer, P. Gagnon, "Assessing the potential of battery storage as a peaking capacity resource in the United States," Applied Energy, Volume 275, 2020, 115385, ISSN 0306-2619, https://doi.org/10.1016/j.apenergy.2020.115385.

[27] NERC Resources Subcommittee, *"Balancing and Frequency Control,"* Princeton, 2011.

[28] P. Denholm, J. Jorgenson, T. Jenkin, D. Palchak, *"The Value of Energy Storage for Grid Applications The Value of Energy Storage for Grid Applications,"* Contract. 303, January, 2013.

[29] J. Eyer, C. Garth, *"Energy storage for the electricity grid: Benefits and market potential assessment guide."* Sandia National Laboratories October, 2010.

[30] N. Padmanabhan, M. Ahmed and K. Bhattacharya, *"Battery Energy Storage Systems in Energy and Reserve Markets,"* in IEEE Transactions on Power Systems, vol. 35, no. 1, pp. 215-226, Jan. 2020, doi: 10.1109/TPWRS.2019.2936131.

[31] M. S. Ziegler, J. E. Trancik, *"Re-examining rates of lithium-ion battery technology improvement and cost decline",*, Volume 14, Issue 4, March, 2021.

[32] W. Kim, J. Shin and J. Kim, *"Operation Strategy of Multi-Energy Storage System for Ancillary Services,"* in IEEE Transactions on Power Systems, vol. 32, no. 6, pp. 4409-4417, Nov. 2017, doi: 10.1109/TPWRS.2017.2665669

[33] NCSS Statistical Software, *"Distribution (Weibull) Fitting,"* Chapter 550, 2012.

[34] M. Jaganmohan, *"Average installed cost for solar photovoltaics worldwide from 2010 to 2020,"* Statista, July, 2021.

[35] S. Vashishta, *"Differentiate between the DNI, DHI, and GHI"* firstgreenconsulting.wordpress.com, May, 2012. [Online]. Available: https://firstgreenconsulting.wordpress.com/2012/04/26/differentiate-between-the-dni-dhi-and-ghi/

[36] SolarSena, *"Solar elevation angle - calculating altitude of sun,"*, April, 2021. [Online]. Available: https://solarsena.com/solar-elevation-angle-altitude/